Article

Not peer-reviewed version

Performance of Self-Sensing Cementitious Composite under Various Loading Conditions

Mohammad Jawed Roshan * , Mohammadmahdi Abedi , António Gomes Correia , Raul Fangueiro

Posted Date: 2 February 2024

doi: 10.20944/preprints202402.0128.v1

Keywords: Piezoresistive performance, loading condition, self-sensing, cementitious composite

Preprints.org (www.preprints.org) | NOT PEER-REVIEWED | Posted: 2 February 2024 doi:10.20944/preprints202402.0128.v1

Article

Performance of Self-Sensing Cementitious Composite under Various Loading Conditions

Mohammad Jawed Roshan [1,*], Mohammadmahdi Abedi [1], António Gomes Correia [1] and Raul Fangueiro [2]

[1] Department of Civil Engineering, ISISE, ARISE, University of Minho, Campus de Azurém, 4800-058 Guimarães, Portugal; agc
[2] Department of Textile Engineering, Centre for Textile Science and Technology, University of Minho, Campus de Azurém, 4800-058 Guimarães, Portugal
* Correspondence: jroshan2020@gmail.com

Abstract: Numerous elements, such as the composition and characteristics of carbon nanomaterials, the composition and characteristics of the matrix material, moisture levels, temperature, and loading circumstances, influence the piezoresistive behaviour of self-sensing cementitious composites. While some past research has explored the impact of some of these factors on the performance of self-sensing cementitious composites, additional investigations need to be conducted to delve into how loading conditions affect the sensitivity of self-sensing cement-stabilized composites. Therefore, this study explores the influences of various loading conditions (i.e., location of loading regarding the location of recording electrodes, and loading level) on the electromechanical performance of self-sensing cement-stabilized sand. To this end, firstly, the evaluation of the percolation threshold based on 10% cement-stabilized sand specimens containing various multiwall carbon nanotubes (MWCNTs) and graphene nanoplatelets (GNPs) was performed. Then, 10% cement-stabilized sand containing 4% MWCNTs/GNPs was tested under various cyclic compressive stresses. The results suggested that the distance between the loading area and the electrode location used for recording the electrical resistance significantly impacts the sensitivity of cement-stabilized sand. Optimal sensitivity was achieved when the electrodes were positioned directly beneath the loading area. Moreover, the study yielded that the stress sensitivity of self-sensing cement-stabilized sand increases proportionally with the stress level. Examination through scanning electron microscopy (SEM) demonstrated that the loading condition influences the bridging characteristics of carbon nanomaterials in cement-stabilized sand, leading to diverse electromechanical behaviors based on the loading condition. This study underscores the importance of considering specific parameters when designing the application of self-sensing cement-stabilized sand for practical field use.

Keywords: piezoresistive performance; loading condition; self-sensing; cementitious composite

1. Introduction

The structural failures caused by different factors, including environmental factors, operational conditions, and extensive loading, result in severe economic losses and safety risks. Although various soil improvement techniques are utilized, the failure of geotechnical infrastructures, even in improved condition, has also been reported [1–3]. Therefore, continually monitoring civil engineering infrastructures is essential to increase service life and enhance safety through early detection and identification of detrimental conditions. To this end, structure health monitoring (SHM) has been employed through diverse systems for the real-time assessment of civil infrastructure conditions. Among other systems, self-sensing cement-based materials have been widely used as SHM systems to detect degradation, cracks, and damage under stress/strain in civil engineering infrastructures. The wide usage of multifunctional cementitious composites is attributed to their advantages such as excellent mechanical and durability properties, low cost, high gauge factor, and considerable compatibility with civil engineering elements [4]. In addition, conventional methods can provide local surficial information about the structural condition, while self-sensing cementitious composites enable the overall integrity of structures; hence, this is a considerable advantage.

To establish the sensing capability, various conductive fillers, including steel fibres [5–8], micro- and nanocarbon fibres [9–12], carbon black [13–16], carbon nanotubes [17–21], graphene nanoplatelets [22–27], steel fibres [28,29], and hybrid conductive fillers [30–33], have been incorporated into cementitious composites. However, carbon-based functional materials have vastly increased cementitious composite piezoresistivity and enhanced mechanical characteristics [34,35]. The change in electrical resistance under induced stress and strain provides the concept of structural health monitoring (SHM) in applying the self-sensing cementitious concept. The self-sensing capability performance level of self-sensing cementitious composite depends on diverse factors, including the type of matrix material (i.e., nonconductive part), water content, binder types, electrode type, electrode configuration, type of conductive fillers, surface condition of conductive fillers, percentage of conductive fillers, dispersion quality, type of electrical circuit, and loading conditions. For instance, the self-sensing cement mortar exhibits better piezoresistive performance than the self-sensing concrete due to the existence of small pores between particles. The micropore condition will affect the resistivity of self-sensing cementitious composites as well. In this regard, Liu et al. [31] reported an increase in electrical resistivity with decreasing moisture content. This issue can be attributed to the emergence of insulated space in the micropores due to decreasing moisture content. To decrease the emergence of micropores during casting, Choi et al. [36] employed various concentrations of defoamer for CNT cementitious composites. Their findings revealed decreased electrical resistance with increasing defoamer concentration due to suppressed voids. The agglomeration of CNTs is another factor that causes porosity in cementitious composites, thus resulting in decreased piezoresistive performance and mechanical strength. To tackle this challenge, the use of silica fume in self-sensing cementitious composites was investigated [34]. The subsequent findings revealed the increasing dispersion of CNTs in cementitious composites with increasing silica fume, thus resulting in increased piezoresistivity and mechanical strength with increasing silica content.

The influence of various factors on the piezoresistive performance of self-sensing cementitious composites has been investigated in previous studies [37–41]. Yıldırım et al. [38] explored the influence of curing time and loading conditions (i.e., four-point bending, tensile, and uniaxial compression). Zhan et al. [39] investigate the influence of conductive filler concentration on piezoresistive performance. Meng et al. [42] evaluated the effects of conductive filler types and aging on the piezoresistive performance of self-sensing cementitious composite. The sensing capability of self-sensing cementitious composites in sensor, coating, and bulk forms was investigated under diverse loadings [43–46]. However, in most previous studies, compressive cyclic and monotonic loadings were applied directly on top of electrodes [14,45,47,48], which differs from some of the real scenarios in civil engineering infrastructures, in which loading may not be directly applied on top of electrodes. Previous research studies only evaluated the influence of loading type (i.e., compressive, tensile, bending, cyclic, and monotonic) on piezoresistive performance [11,38,41,42,49,50]. Therefore, although the sensing capability of self-sensing cementitious composites is undeniable, the effects of loading conditions (i.e., location of loading regarding location of recording electrodes and loading level) on the sensing capability of cementitious composites still need to be fully comprehended. To this end, the current study investigates the performance of self-sensing cement-stabilized sand containing 4% MWCNT/GNP under various compressive cyclic loading conditions. The hybrid MWCNT/GNP was utilized to minimize the micropores and, accordingly, to increase the electromechanical performance of self-sensing cement-stabilized sand [51]. The electromechanical tests were conducted under various cyclic compressive loadings to consider the loading conditions in transportation infrastructures. The current study's findings provide information regarding the effects of loading conditions (i.e., location of loading regarding the location of recording electrodes, and loading level) on the electromechanical properties of self-sensing cement-stabilized sand that need to be considered before application in field projects. The findings of this research can be helpful in carefully arranging and configuring the electrodes used for the electrical signals collection in a self-sensing cementitious composite system.

2. Material and methods

2.1. Materials

The relevant materials are categorized into matrix and conductive/functional materials in self-sensing cementitious composites. In the first step, the effects of adding various MWCNT/GNP concentrations on the impedance of cement-stabilized sand were evaluated using a PalmSens device. Based on the findings, further analyses to evaluate the effects of loading conditions on the piezoresistive performance of self-sensing cement stabilized sand were conducted only on specimens containing 4%MWCNT/GNP. To stabilize the sand for being applied in transportation infrastructure sublayers, 10% ordinary Portland cement (OPC) was utilized. The porosity distribution is one of the main factors affecting the electromechanical characteristics of self-sensing cementitious composites [36]. Given this issue, standard sand was used in this study to minimize the effects of particle size and nonhomogeneous distribution of porosity on the electromechanical properties of cement-stabilized sand. The grain size distribution (GSD) of ordinary Portland cement (OPC) and standard sand are depicted in Figure 1 according to EN 196–1, ISO 679: 2009, and EN 197/1-2011 standards [52]. Further details on the GSD and physical properties of the standard sand used in this study are tabulated in Table 1.

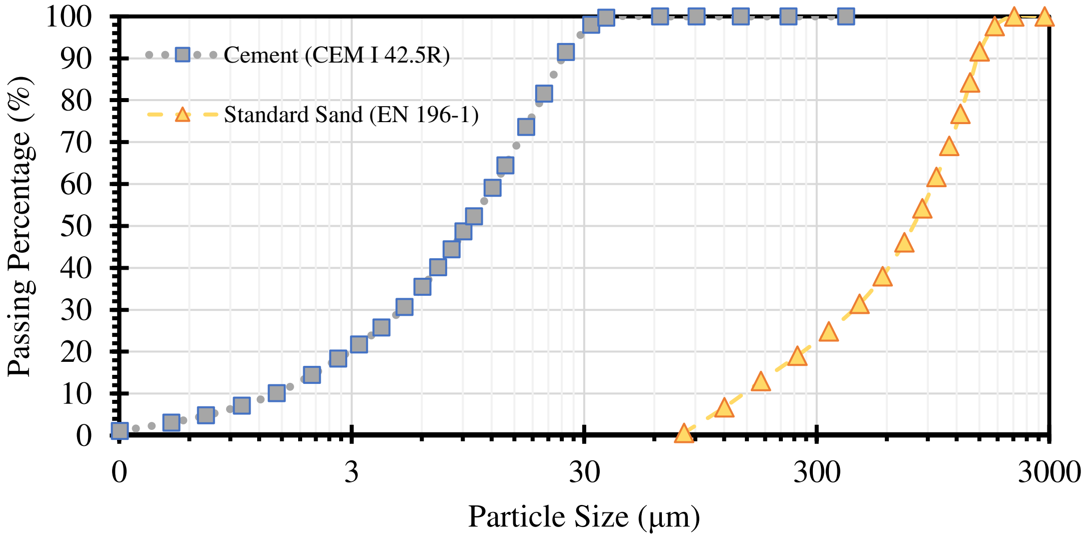

Figure 1. Grain size distribution of standard sand and ordinary Portland cement.

Table 1. Physical properties of standard sand.

Mesh Size (mm)	0.08	0.16	0.5	1	1.6	2
Cumulative retained (%)	99±5	87±5	67±5	33±5	7±5	0
Specific gravity	2.67		Uniformity coefficient =7.5		Curvature coefficient = 1.8	

Depending on the composition, cement is categorized into over ten types [53]. However, in the current study, ordinary Portland cement (OPC) CEM 1, 42.5R was used as a binder agent due to its low cost, high effectiveness, considerable workability and density, progressive strength gain, and excessive resistance to chemical reactions. Given these features, this type of cement is commonly used to improve transportation infrastructures [54]. The chemical and physical properties of CEM 1 and 42.5R employed in this study are presented in Table 2.

Table 2. Chemical and physical properties of CEM 1, 42.5R.

SiO2	Al2O3	Fe2O3	MgO	CaO	Na2O	TiO2	K2O	MnO	P2O5	SO3
19.94	4.76	3.38	1.31	63.93	0.17	0.24	0.44	0.075	0.063	2.54
Loss on Ignition (LOI			Fineness (m2/kg)				Specific Gravity			
2.97			360				3.15			

Diverse functional materials have been used in previous studies [55] to establish the sensing capability in cementitious composites. In the current study, hybrid carbon nanomaterials comprising MWCNTs and GNPs were utilized due to their remarkable synergistic effects on the mechanical and electromechanical characteristics of self-sensing cementitious composites [51]. The details of the MWCNTs and GNPs utilized in this study are tabulated in Table 3.

Table 3. Characteristics of GNPs and MWCNTs

GNP										
Surface Area (m^2 g-1)	Density (g/cm3)	Carbon Content (%)	Tensile Modulus (GPa)	PH Value (30° C)	Tensile Strength (GPa)	Layers	Dimension		Form	Part Number
							Thickness	Diameter		
120-150	0.6	>99.5	1000	7-7.65	5	10< n <60	4-60 nm	5-10 μm	Gray Powder	TGN201
MWCNT										
Surface Area (m^2 g-1)	Density (g/cm^3	Color	Outside Diameter (nm)	Length (μm)	Ash (wt.%)		Carbon Content (%)		Part Number	
350	0.27	Black	<50	10-30	<1.5		>98		GCM327	

The agglomeration of carbon nanomaterials due to their massive specific surface area and energy is one of the main concerns in self-sensing cementitious composite fabrication. To tackle this challenge, dispersion techniques, including physical and chemical techniques, have been applied in previous studies [10,56]. In the current study, combined physical (i.e., sonication) and chemical (i.e., the addition of Pluronic F-127 into water) methods were employed to achieve the desired dispersion of MWCNT/GNP in water. In addition, to avoid foam formation due to the chemical reaction of the surfactant (Pluronic F-127), tributyl phosphate 97% was also used as a foam reducer.

2.2. Mixing procedures and sample preparation

Although the general fabrication procedures for self-sensing cementitious composites are similar to those of conventional cementitious composites, a few extra steps, including the dispersion of carbon nanomaterials and the installation of electrodes, are necessary for the fabrication of self-sensing cementitious composites. In the first step, therefore, 10% surfactant (Pluronic F-127) by weight of carbon nanomaterial and 50% TBP-97% by weight of surfactant were thoroughly dissolved in water (i.e., optimum moisture content). Then, 0.5%, 1%, 2%, 3%, and 4% MWCNT/GNP (1:1) by weight of dry sand was added to the obtained solution, and after thoroughly stirring and mixing, bath sonication was employed to disperse the CNMs in solution. It should be noted that the combined dispersion technique (i.e., using Pluronic F-127 and sonication) used in the current study has been proven to be suitable for the dispersion of carbon nanomaterials in 2015 by Parveen et al. [57]. The dispersed CNMs were then added to the dry mixed sand and cement. The self-sensing cementitious composite components were thoroughly mixed in the mixer. Finally, samples with dimensions of 160 mm*40 mm*40 mm were fabricated according to the maximum dry density, which is usually considered for the compaction of the transportation layer. The prepared samples were tested after 28 days of curing in a humid room. The steps followed for mixing the self-sensing cementitious composite and sample preparation are summarized as illustrated in Figure 2.

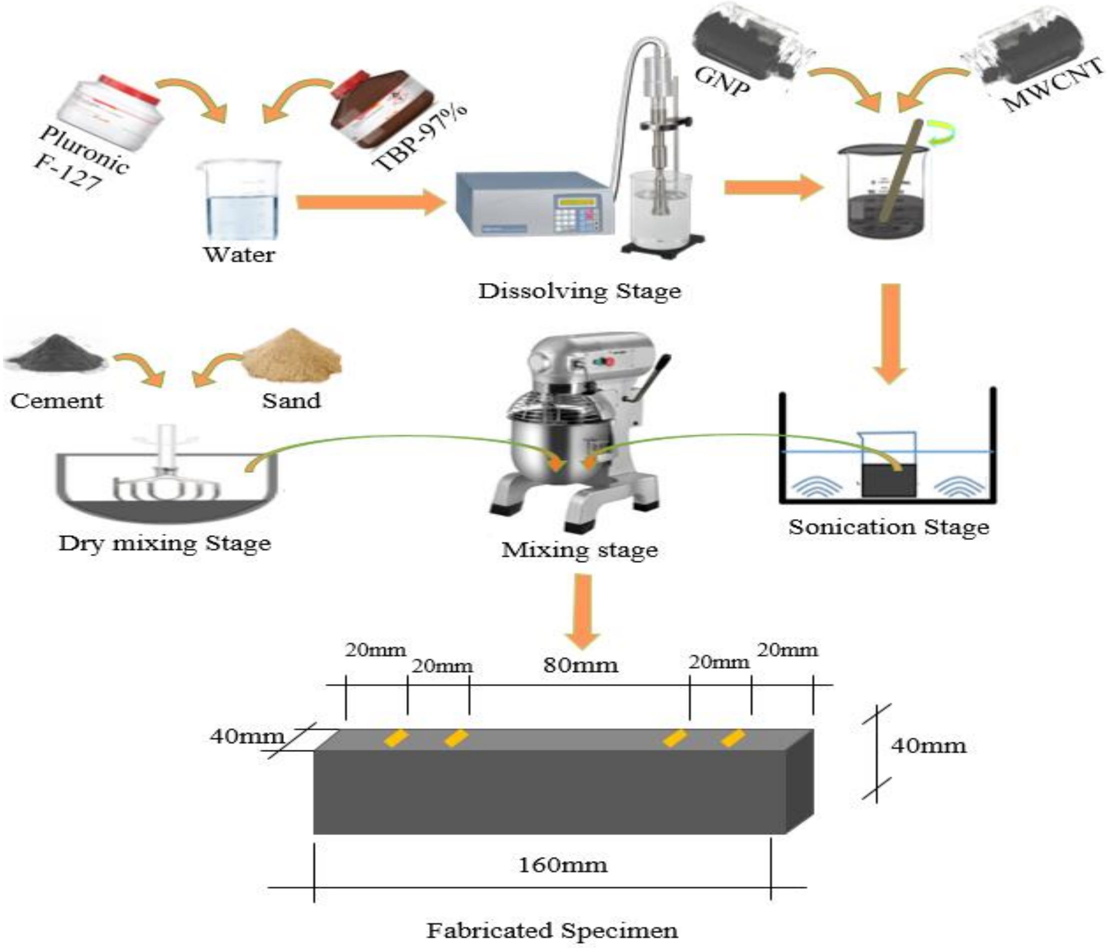

Figure 2. Mixing and sample fabrication stages.

2.3. Experimental methods

In the first step, the influence of adding various MWCNT/GNP on electrical impedance was evaluated using a PalmSens device. Then, further investigations were conducted on the specimens containing 4% MWCNT/GNP. In most previous studies, the electromechanical characteristics of self-sensing cementitious composites have been investigated under the loading conditions shown in Figure 3e [23,58,59]. In this study, an electromechanical test was conducted under various compressive cyclic loading conditions to evaluate the sensing capability of the bulk self-sensing cementitious composite, as shown in Figure 3. Five scenarios shown in Figure 3 were considered for electromechanical testing. With the loading conditions shown in Figures 3a and b, cyclic compressive loading was applied to the region between electrodes, and the electrical resistance was recorded from the inner and outer electrodes. In Figure 3c, cyclic compressive loading was exerted on the region between electrodes, and the electrical resistance was measured through the inner electrodes. The exact loading level and shape used in Figure 3c were executed on top of the electrodes in Figure 3d, and the electrical resistance was recorded from those electrodes under the loading region. In the last loading scenario, various compressive cyclic loading levels were applied to evaluate the effects of loading level on the piezoresistive performance of the self-sensing cementitious composite.

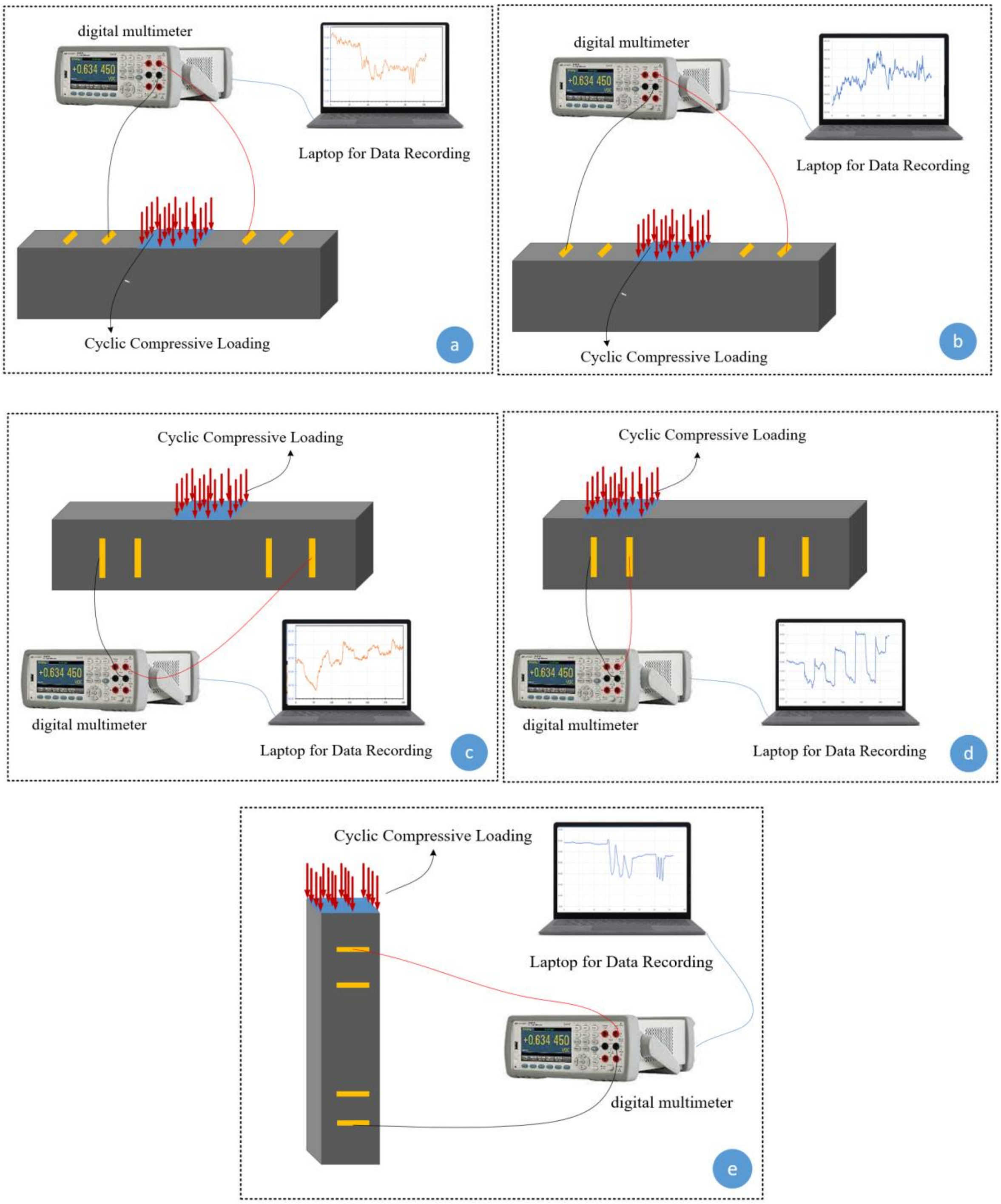

Figure 3. Various applied loading conditions (a, b, c, d, e) for piezoresistive performance measurement.

In addition to the electromechanical test, microstructural characteristics were evaluated based on scanning electron microscopy (SEM) experiments to appraise the influence of MWCNT/GNP on the morphology of cement-stabilized sand. The specimens for SEM analysis were prepared from the collapsed electromechanical testing sample. The SEM samples were coated with Au–Pd thin film (30 nm) using a high-resolution sputter coater (Cressington 208HR). Following the coating stage, the SEM experiment was conducted using 10 kV voltage and secondary electron mode.

2.4. Piezoresistivity measurements

The electrical resistance was recorded using an Agilent 34461A 6½ Digit digital multimeter during the loading scenarios mentioned above. The recording rate was adjusted to 10 times per second to thoroughly capture the electrical resistance under loading. Although the samples were cast with four electrode probes, a two-probe system with DC current was employed to record the electrical resistance in this study. The fractional changes in resistivity (FCR) were calculated according to Equation 1.

$$FCR = \frac{\Delta R}{R_0} \approx \frac{\Delta \rho}{\rho_0} \tag{1}$$

where ΔR, $\Delta \rho$, R_0, and ρ_0 are the fractional changes in resistance, fractional changes in resistivity, initial resistance, and initial resistivity, respectively. The changes in resistance after applying the load are schematically illustrated in Figure 4. Figure 4 shows that the resistance can increase or decrease depending on the integrity condition of the self-sensing cementitious composite under loading.

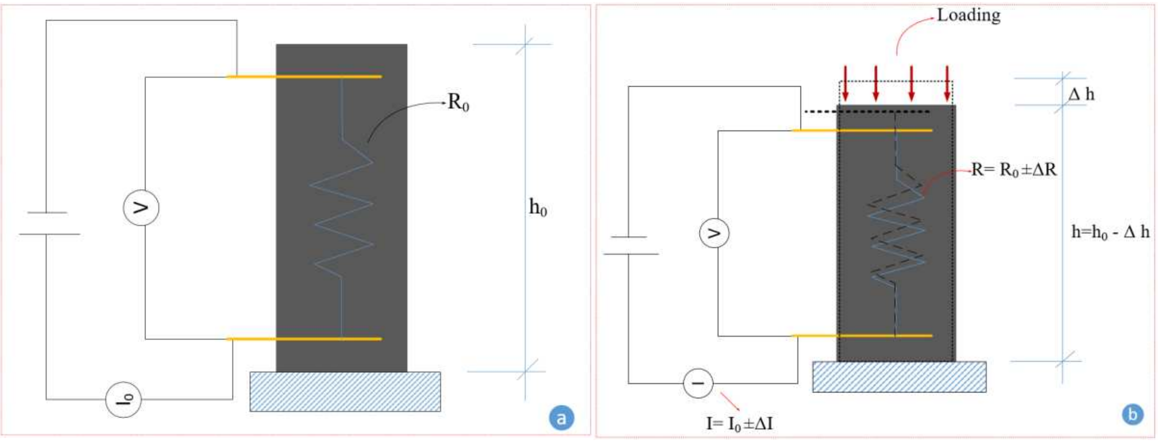

Figure 4. Electromechanical concept under compressive loading: a) initial resistance b) resistance changes under loading.

3. Results and discussion

3.1. Influence of MWCNT/GNP concentration on electrical impedance

In the current study, a PalmSens device, which works based on AC, was employed to evaluate the influence of conductive fillers on the impedance of 10% cement-stabilized sand. Adding MWCNT/GNP in cement-stabilized sand produces random conductive pathways, resulting in decreased electrical impedance, as seen in Figure 5. Figure 5a illustrates the recorded electrical impedance over 120 sec for specimens containing various MWCNT/GNP concentrations ranging from 0% to 4%. Regarding Figure 5a, it is seen that the electrical impedance decreases with increasing MWCNT/GNP concentrations. Figure 5b was plotted according to Figure 5a to evaluate the influence of MWCNT/GNP concentrations on the electrical impedance of 10% cement stabilized sand, a construction material usually used in transportation infrastructures sublayers. Figure 5b indicates the drastic decrease in electrical impedance after adding 1%MWCNT/GNP, indicating the percolation threshold. The reduction rate in electrical impedance of 10% cement stabilized sand decreases with increasing MWCNT/GNP beyond 1%. This issue is attributed to the concentration of forming conductive pathways originating from adding conductive fillers. In other words, the conductive pathways in 10% cement stabilized will not be significant when the concentration of MWCNT/GNP is lower than 1%, resulting in a large electrical impedance. However, when the concentration of MWCNT/GNP is more than 1%, the electrical impedance is small due to the produced intensive conductive pathways within 10% cement-stabilized sand. Since the objective of this study is to evaluate the effects of loading conditions on piezoresistive performance of self-sensing cement stabilized sand, 4%MWCNT/GNP was incorporated in 10% cement stabilized specimens used for further analysis. This way, the highly sensitive cement-stabilized sand can be produced, minimizing the polarization effects during testing.

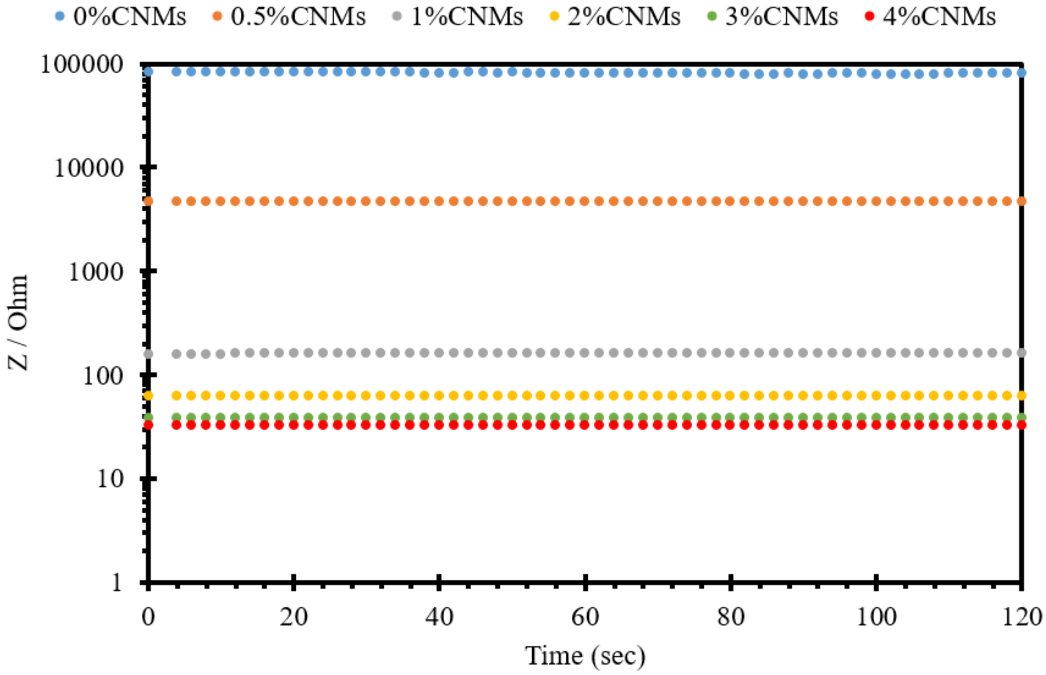

(a)

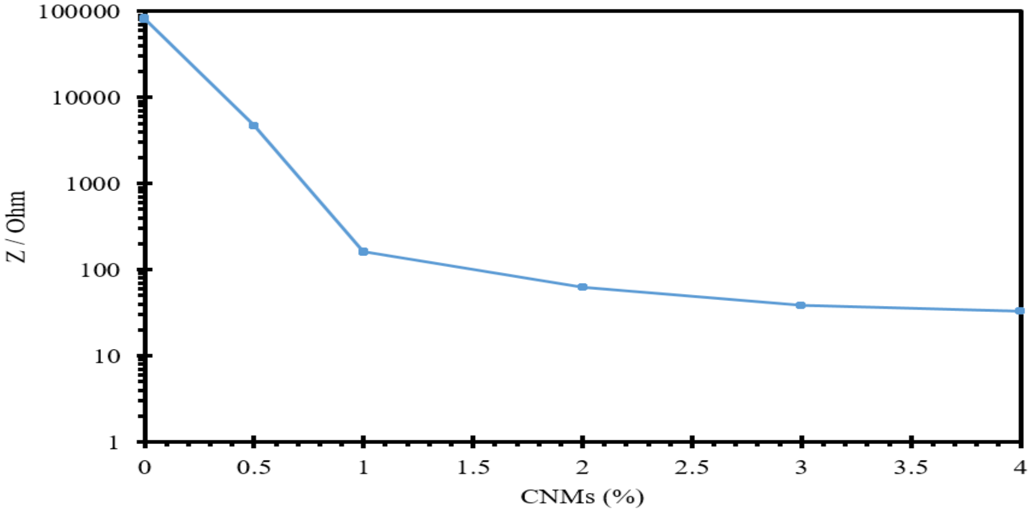

(b)

Figure 5. a) Electrical impedance-time of self-sensing cement stabilised sand containing various percentage of CNMs (MWCNT/GNP) b) Electrical impedance-CNMs (MWCNT/GNP).

3.2. Effects of distance of loading region from electrodes on piezoresistive performance

The piezoresistivity of the self-sensing cementitious composite is the electrical resistance changes due to stress, strain, and damage. The stress, strain, and damage-sensing ability of self-sensing cementitious composites have been explored widely in previous studies [10,60–62]. However, in previous studies, loading was directly applied on top of electrodes [14,63–65]. Given this issue, this section discusses the influence of the loading region distance from the electrodes used for electrical resistance recording on the piezoresistive performance. Figure 6 illustrates the FCR changes for the loading conditions shown in Figures 3a and b. The blue line represents the cyclic compressive stress, and the black and yellow lines indicate the FCR changes for conditions a (close to the loading region) and b (far from the loading region), respectively, shown in Figure 3. Comparing the FCR changes in Figure 5 under the same stress level yields the conclusion that the loading distance from the electrodes used for the electrical resistance recording significantly affects the piezoresistive performance of self-sensing cementitious composites. For instance, in Figure 6a, it is seen that the FCR changes under the loading condition of Figure 3a are evident compared to those in the loading condition of Figure 3b.

Similarly, the differential response of FCR under compressive cyclic stress is obvious for the loading conditions of Figure 3a and b in Figures 6 b and c. Therefore, it is concluded that the stress sensitivity of the self-sensing cementitious composite is affected by the loading distance from the electrodes used for electrical resistance recording. In addition, Figure 6 shows that the stress sensitivity increases with increasing stress levels from 272 kPa to 520 kPa and 643 kPa. However, the FCR changes with increasing stress level only become evident for the inner electrodes (condition a). The stress sensitivity for the outer electrodes did not appear under the maximum stress used in this part (643 kPa). Given the issues discussed, it is important to consider the effects of the loading region on the stress sensitivity of self-sensing cementitious composites before applying them in a real-world project. The electrode location employed for electrical resistance recording plays a vital role in the stress sensitivity of self-sensing cement-stabilized sand.

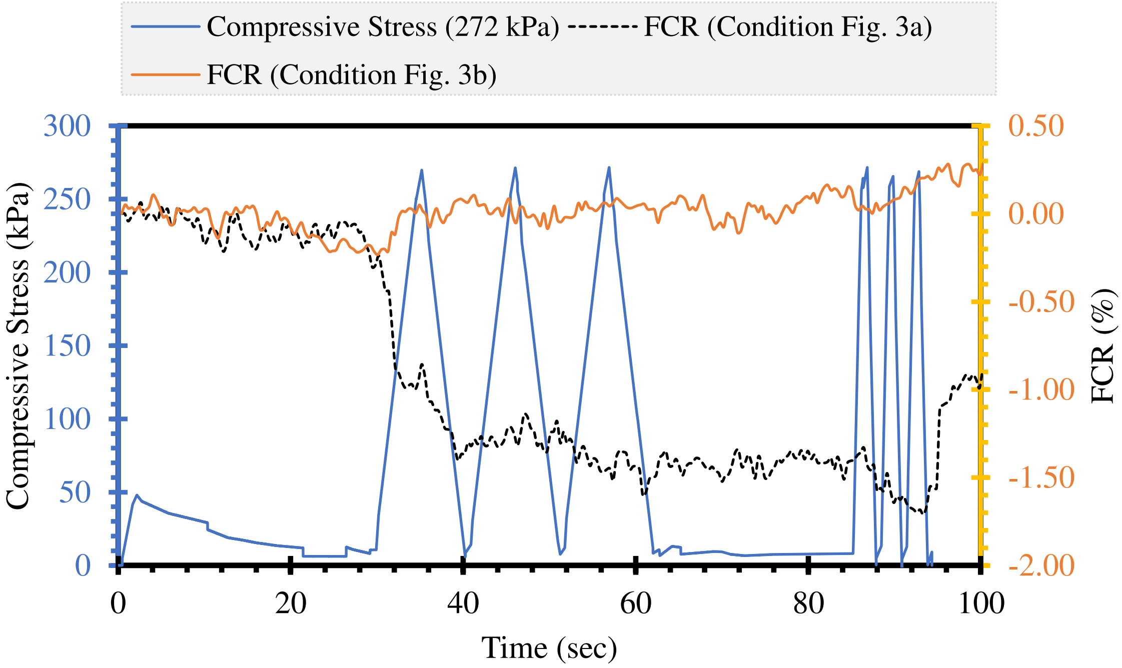

(a)

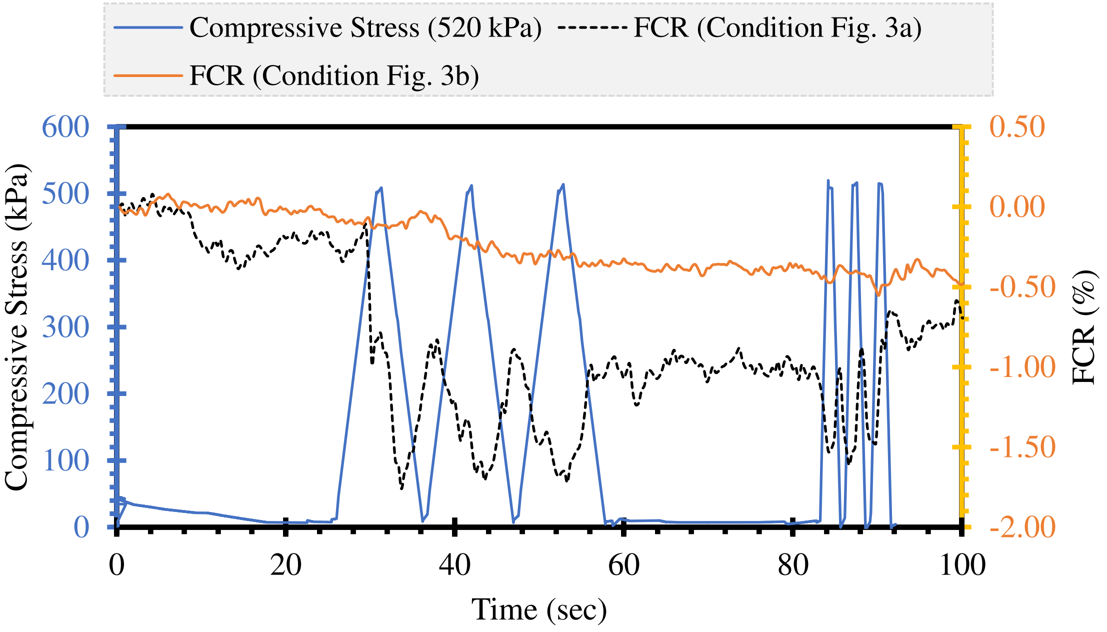

(b)

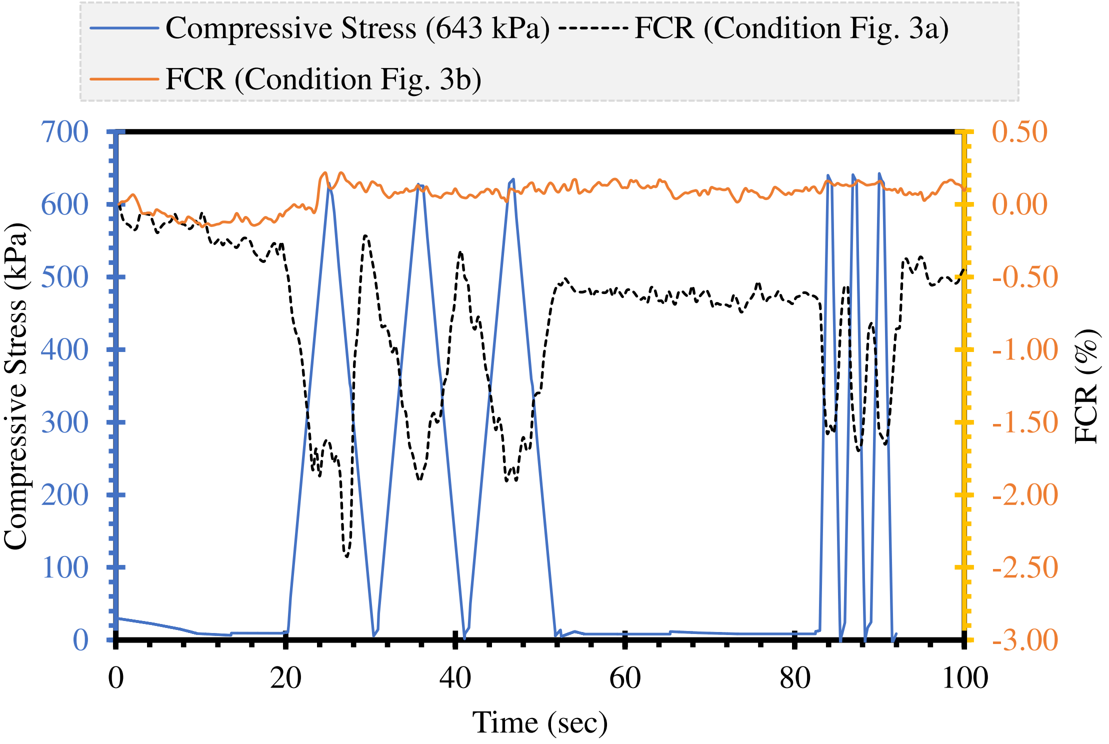

(c)

Figure 6. Compressive cyclic stress/FCR-time for loading conditions according to Figure 3a,b; a) Cyclic compressive stress=272 kPa; b) Cyclic compressive stress=520 kPa; c) Cyclic compressive stress=643 kPa.

3.3. Effects of loading position on piezoresistive performance

To further evaluate the piezoresistive performance of self-sensing cement-stabilized sand with respect to loading conditions, three compressive cyclic stress levels (313 kPa, 628 kPa, and 1,268 kPa) were applied to self-sensing cementitious samples according to Figures 3c and d. Figure 7 depicts the FCR changes under cyclic stress for the loading conditions in Figure 3c (loading on the region between electrodes) and Figure 3d (loading on top of electrodes). In the case of the loading condition in Figure 3c (loading on the region between electrodes), in which the electrical resistance was recorded from the outer electrode, the FCR changes under compressive stress are not readily noticeable, as seen in Figure 7 in yellow. In contrast, the FCR trends obtained for the loading condition in Figure 3d (loading on the top of electrodes) follow the compressive stress, as shown in black in Figure 7. This behaviour is attributed to the conductive pathways that emerge under compressive loading. In the case of the loading condition in Figure 3c, the conductive pathways that emerge under loading are not contiguous, and electrical conduction disruption occurs between electrodes because they are situated far from the loading region. On the other hand, continuous conductive networks occur between two electrodes under loading conditions, as shown in Figure 3d, since the loading area covers the region between electrodes. In other words, the covering of electrodes by the loading area causes increased conductive networks between two electrodes upon decreased gaps between functional fillers, resulting in increased stress/strain sensitivity of self-sensing cement-stabilized sand. These findings indicate the importance of the electrode layout for successfully applying self-sensing cement-stabilized sand. Considering the loading region, if the electrode position is not selected mindfully, the stress-sensing capability of self-sensing cement-stabilized sand, particularly under low stress levels, will be insignificant. Therefore, when self-sensing cement-stabilized sand is used in bulk form, the distance and number of electrodes used to collect electrical resistance data play a crucial role in successfully applying this intelligent material for stress-sensing purposes. Given this issue, the sensitivity of self-sensing cementitious composites has been widely investigated by installing electrodes directly under stress regions in the laboratory [43,45,66–69] and at field scales [20,70–72] in the literature. The results obtained from the current study regarding the influence of loading position on the piezoresistive performance of self-sensing cementitious composites have been neglected in previous studies; thus, the outputs presented in this study are novel [12,49,73]. The stress sensitivity of self-sensing cement-stabilized sand is considerable when electrodes are directly subjected to stress compared to the cases in which the electrodes are located far from the stress regions. Therefore, it is concluded that the sensitivity of the self-sensing cementitious composite is highly dependent on the location of the electrodes and the loading region.

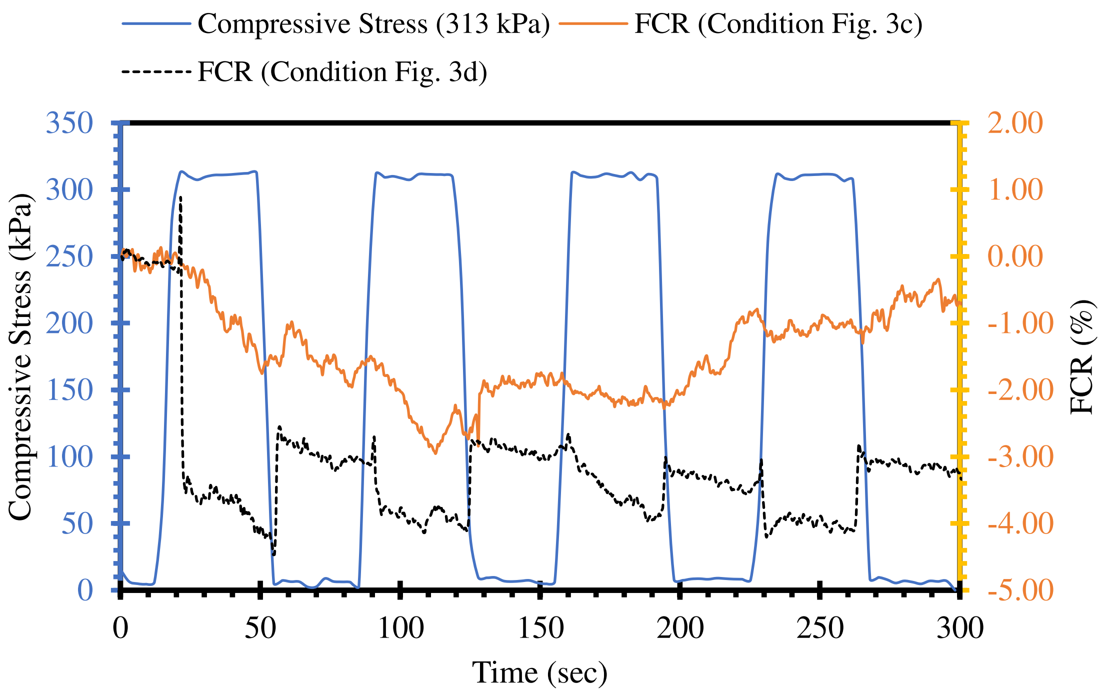
Compressive Stress (313 kPa)
FCR (Condition Fig. 3c)
FCR (Condition Fig. 3d)
Compressive Stress (kPa)
350
300
250
200
150
100
50
0
FCR (%)
2.00
1.00
0.00
-1.00
-2.00
-3.00
-4.00
-5.00
0
50
100
150
200
250
300
Time (sec)

(a)

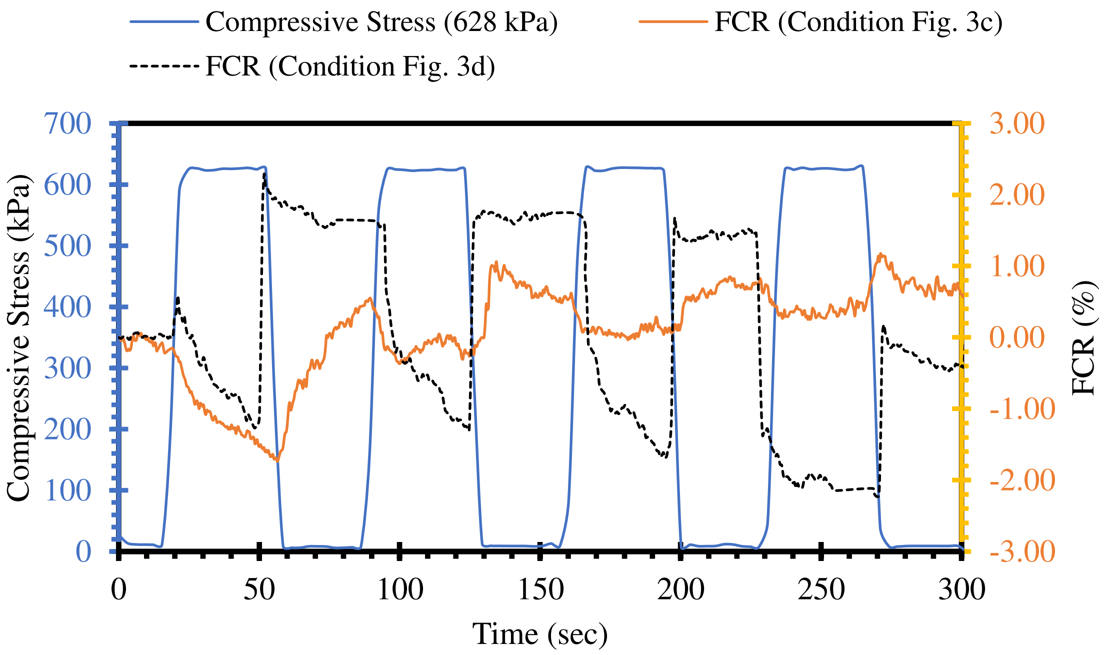
Compressive Stress (628 kPa)
FCR (Condition Fig. 3c)
FCR (Condition Fig. 3d)
Compressive Stress (kPa)
700
600
500
400
300
200
100
0
FCR (%)
3.00
2.00
1.00
0.00
-1.00
-2.00
-3.00
0
50
100
150
200
250
300
Time (sec)

(b)

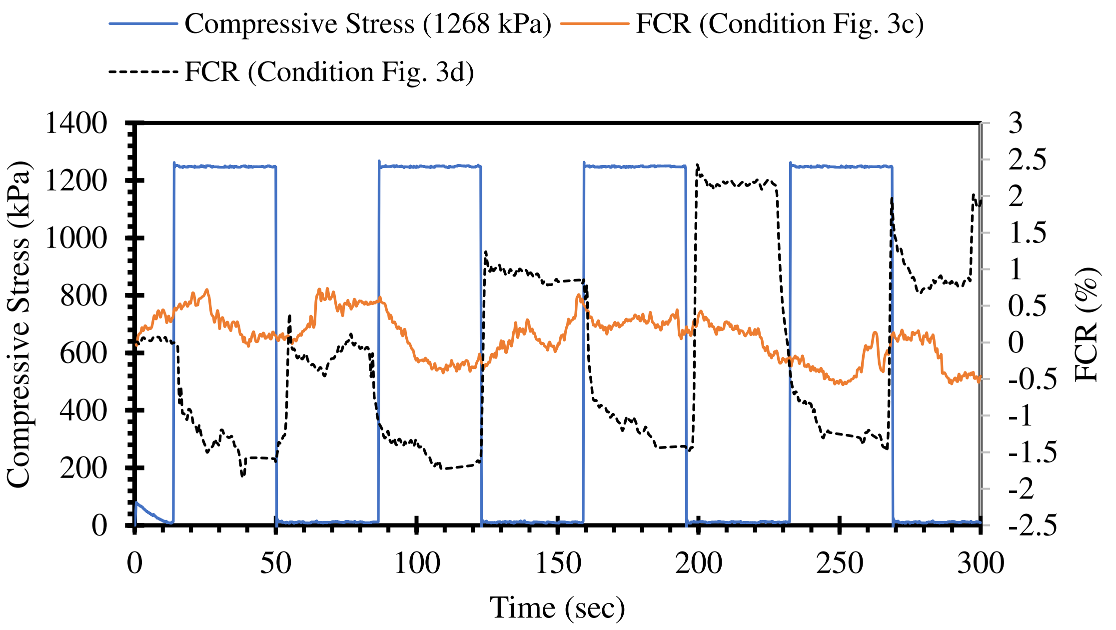

(c)

Figure 7. Compressive cyclic stress/FCR-time for loading conditions according to Figure 3c,d.

3.4. Effects of stress level on piezoresistive performance

Among other factors, the stress level induced by the applied external load is one of the main factors affecting the piezoresistive performance of the self-sensing cementitious composite [74–76]. In this section, the FCR changes of self-sensing cement-stabilized sand containing 4% MWCNT/GNP were evaluated under the loading conditions in Figure 3e by applying various stress levels ranging from 63 kPa to 3,804 kPa, as illustrated in Figures 8 and 9. Figures 8 and 9 illustrate the incremental sensing ability with increasing stress levels. For instance, as seen in Figure 8a, the FCR change trend is unclear under 63 kPa compressive cyclic stress, indicating that the cement-stabilized sand containing 4% MWCNT/GNP lacks the sensitivity to detect actions in the transportation infrastructures field below this stress level. However, a sudden change in FCR is seen in Figure 8a after the first compressive cyclic stress, showing the negligible stress-sensing capability. Although the FCR change trends started following the compressive cyclic stress trend after applying 275 kPa and 527 kPa, this is not evident in Figures 8b and c. The FCR changes yielded an explicit alteration pattern under 1,022 kPa compressive cyclic stress, as seen in Figure 8d.

Similarly, the FCR variations continued to increase with increasing stress level, as shown in Figure 9. The findings in Figures 8 and 9 indicate the considerable effects of stress levels on the sensing capability of self-sensing cement-stabilized sand. The self-sensing cement-stabilized sand could be used in field situations for strain, damage, and traffic detection. This detection using self-sensing cementitious composites would not be possible for low stress levels. However, the damage could be detected by considering the initial and sudden changes in the FCR trend under compressive cyclic stress, even in the case of a small level of stress. Previous studies provided comprehensive information regarding damage detection under cyclic and monotonic loading [51,77]. In addition, it should be noted that the strain-sensing capability of self-sensing cement-stabilized sand is highly dependent on the strain level caused by applied stress. The strain increases with increasing stress levels; hence, the FCR changes become clearer with increasing strain levels. Given this issue, it is clearly evident in Figures 8 and 9 that the FCR decreases during the loading stages and increases during the unloading stages. The loading stages cause the shrinkage of voids and decreased distances between functional fillers, leading to decreasing FCR. The larger the stress level, the more considerable the decrease in FCR would be due to compressed voids and emerging electrical conductive pathways. In general, the results achieved regarding the influence of stress level on the piezoresistive performance of self-sensing cementitious composite in this study are coherent with those of previous studies [23,78,79].

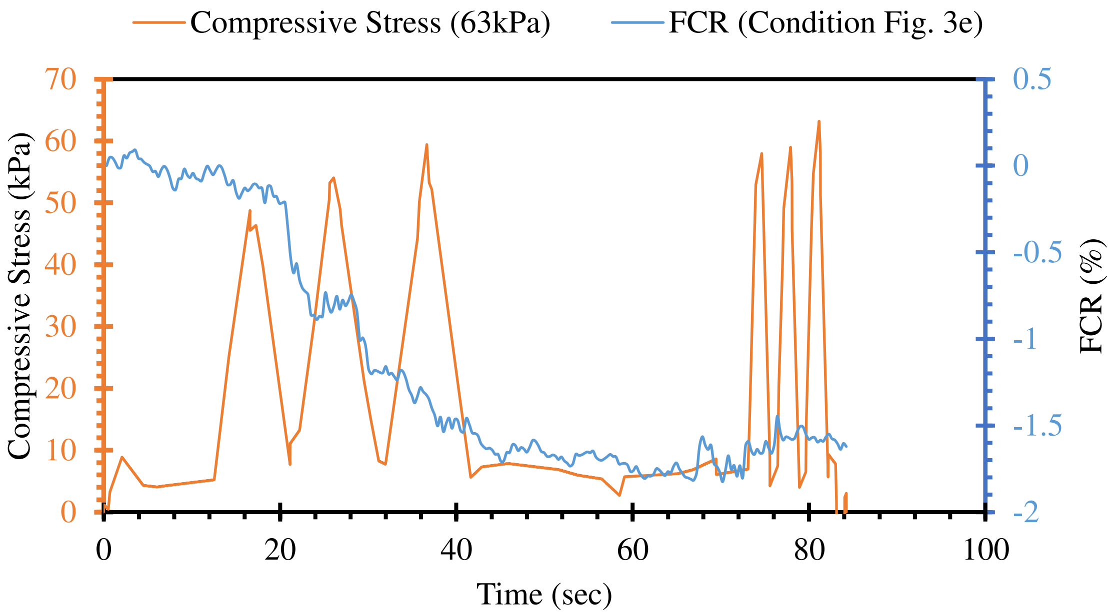

(a)

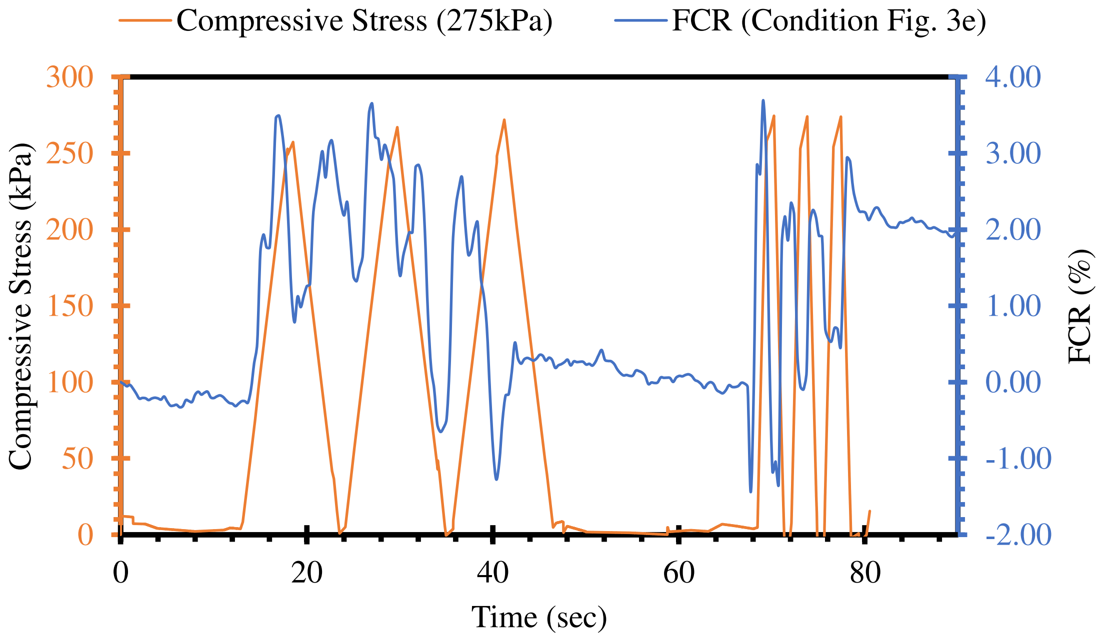

(b)

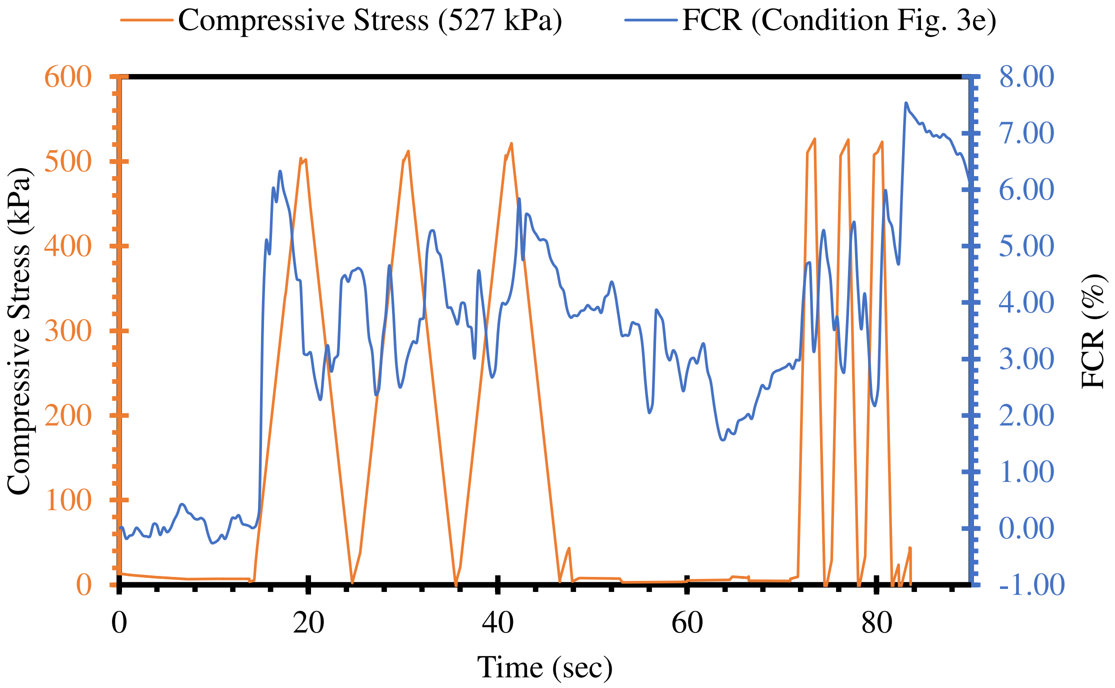

(c)

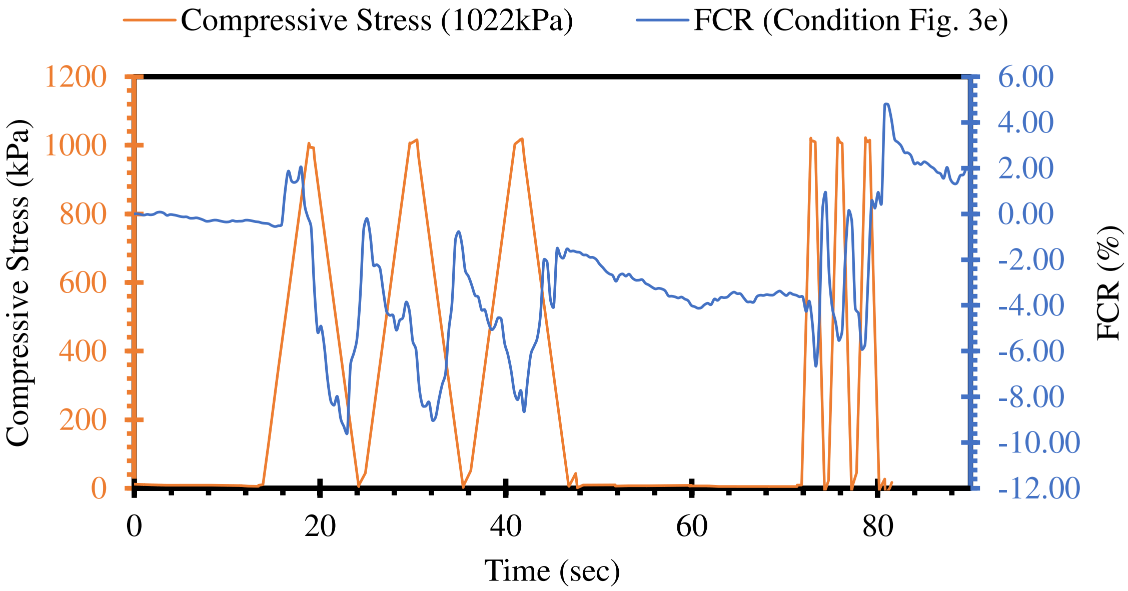

(d)

Figure 8. Compressive cyclic stress/FCR-time for loading conditions under 1,000 kPa according to Figure 3e.

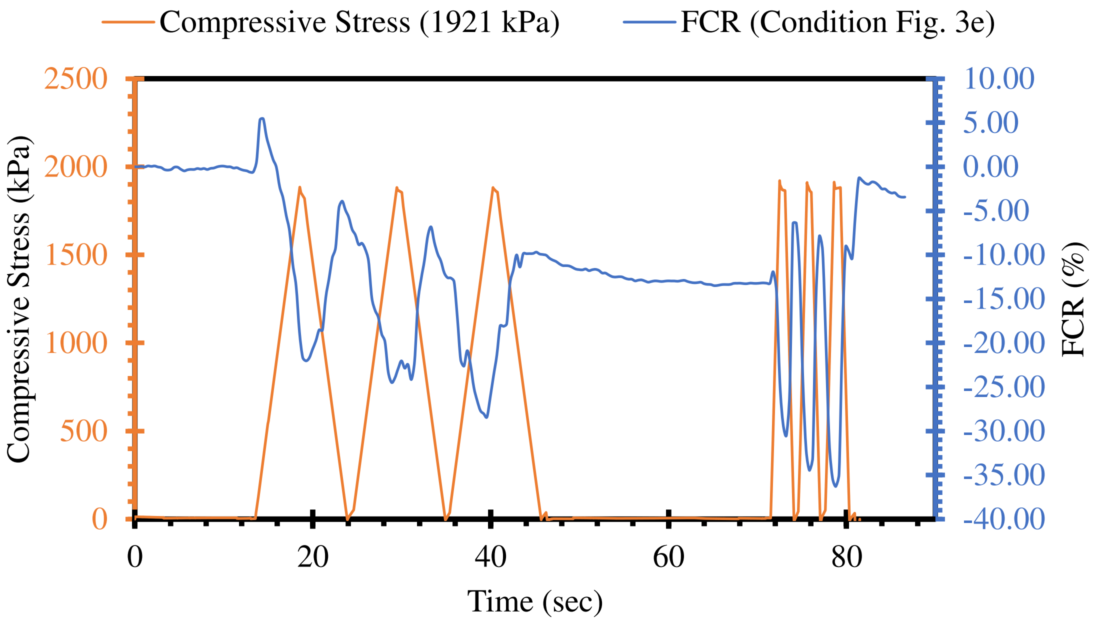
Compressive Stress (1921 kPa)
FCR (Condition Fig. 3e)
Compressive Stress (kPa)
2500
2000
1500
1000
500
0
10.00
5.00
0.00
-5.00
-10.00
-15.00
-20.00
-25.00
-30.00
-35.00
-40.00
FCR (%)
0
20
40
60
80
Time (sec)

(a)

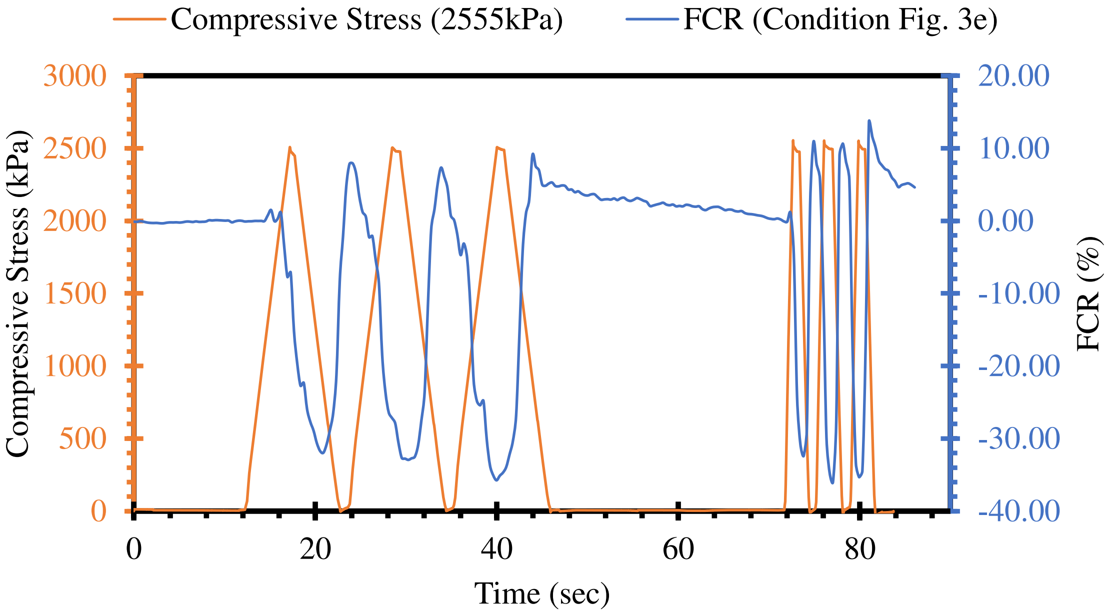
Compressive Stress (2555kPa)
FCR (Condition Fig. 3e)
Compressive Stress (kPa)
3000
2500
2000
1500
1000
500
0
20.00
10.00
0.00
-10.00
-20.00
-30.00
-40.00
FCR (%)
0
20
40
60
80
Time (sec)

(b)

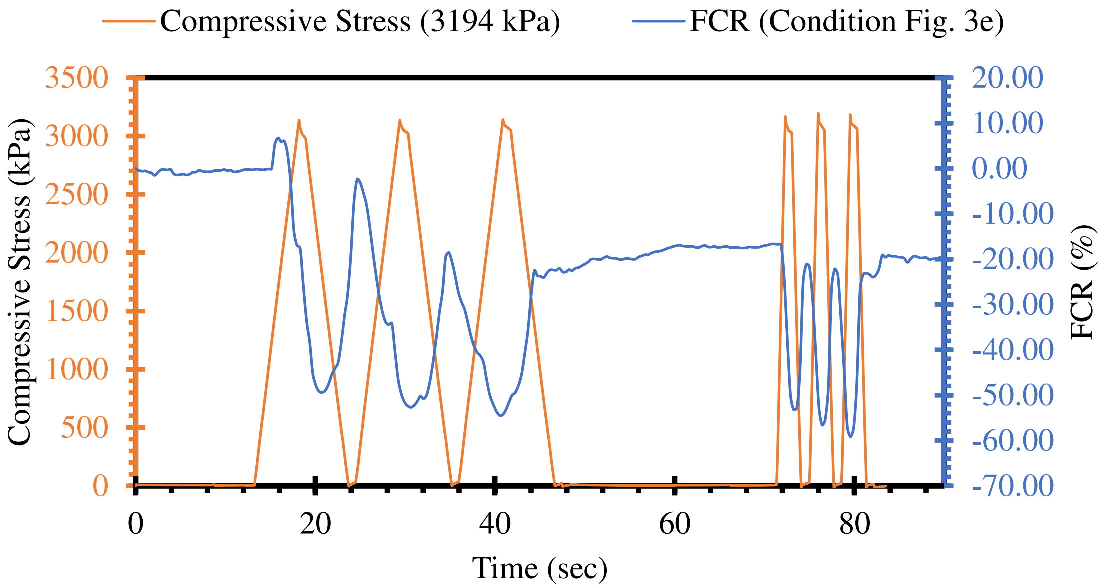

(c)

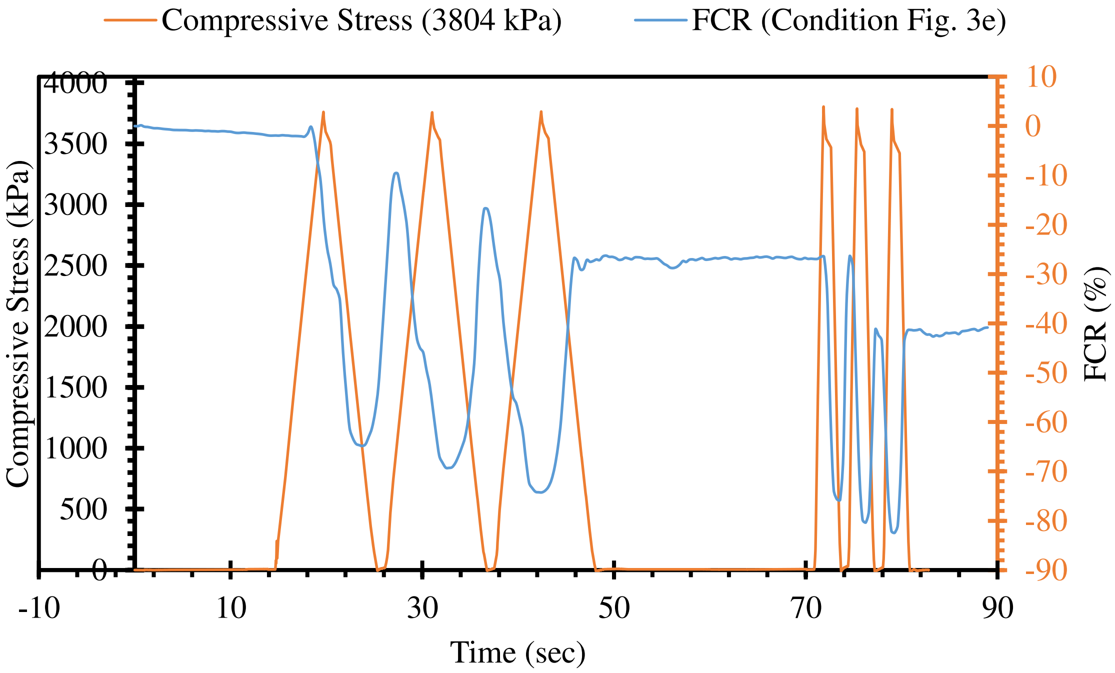

(d)

Figure 9. Compressive cyclic stress/FCR-time for loading conditions over 1,000 kPa according to Figure 4e.

This section discusses the correlation between FCR and stresses for load conditions applied on the small surface of prismatic specimens, as illustrated in Figure 3e. FCR is defined as follows.

$$FCR = \frac{\Delta R}{R_0} \times 100 = f(\sigma_x) \tag{2}$$

As discussed, the FCR decreases and increases under cyclic compressive loading and unloading stages, respectively. However, hysteresis in FCR may occur due to various factors, including the type of components of the self-sensing cementitious composite, temperature variation, and stress level. The FCR changes highly depends on the induced stress level, as seen in Figures 10 and 11. The self-sensing cementitious composite may not be sensitive under a small stress level, as seen in Figure 10a for 63 kPa cyclic compressive stress. In Figure 10a, two separate regions of FCR changes under cyclic compressive stress are evident. In the first portion, sudden changes in FCR occurred under the first three stress cycles, which can also be observed in Figure 8a. In the second region, the change in FCR under cyclic compressive stress is negligible. The drastic changes in FCR in the first region are attributed to the initial accommodation of the cementitious composite and compression of the interface between the electrodes and smart material. After this phase, the stress sensitivity of self-sensing cement-stabilized sand under 63 kPa becomes almost zero in the second region in Figure 10a. This phenomenon can also be observed in Figure 8a, in which the FCR drastically decreases under the first three stress cycles and becomes almost constant under subsequent cycles.

The stress sensitivity of self-sensing cement-stabilized sand started upon increasing the stress level, as seen in Figures 10b, c, d and Figures 11a, b, c, d. Regarding Figure 10b, c, d and Figures 11a, b, c, d, it is observed that the FCR changes increase with increasing stress levels. The increasing trend of FCR changes under increasing compressive cyclic stress indicates enhanced sensitivity performance. However, reversibility is another factor that should be considered in self-sensing cementitious composites. The findings indicate that the self-sensing cement-stabilized sand could not sense the small stress level. Conversely, a linear correlation was achieved between FCR changes and stress levels up to 2,555 kPa (approximately 67% of ultimate strength). Beyond 67% of ultimate strength, a polynomial correlation was established between FCR changes and compressive cyclic stress, as exhibited in Figures 11c and d. The linear correlation between the FCR and compressive cyclic stress indicates the reversibility of FCR and the irreversibility of baseline electrical resistance. This issue can be observed in Figures 8 and 9, where under compressive cyclic stress up to 2,555 kPa, the FCR is almost completely reversible after each loading and unloading, while the baseline resistance is not reversible. Beyond 2,555 kPa, both FCR changes and baseline resistance yielded an irreversible trend, as seen in Figures 9c and d. In previous studies, it has been found that FCR is reversible under cyclic compressive stress up to 75% of ultimate strength, while it would be irreversible when the cyclic compressive stress exceeds 75% of ultimate strength, indicating that the findings are coherent with previous study results [80]. It should be noted that the most considerable repeatability was observed under 2,555 kPa cyclic compressive stress, as seen in Figures 9b and 11b.

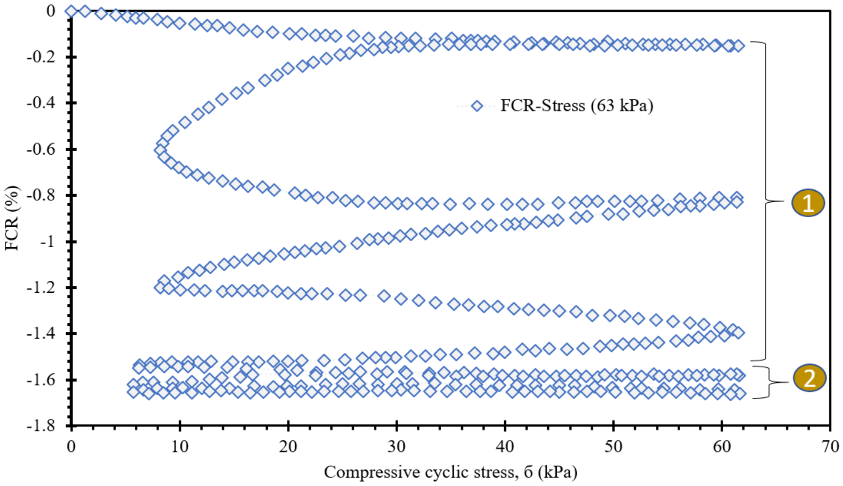

(a)

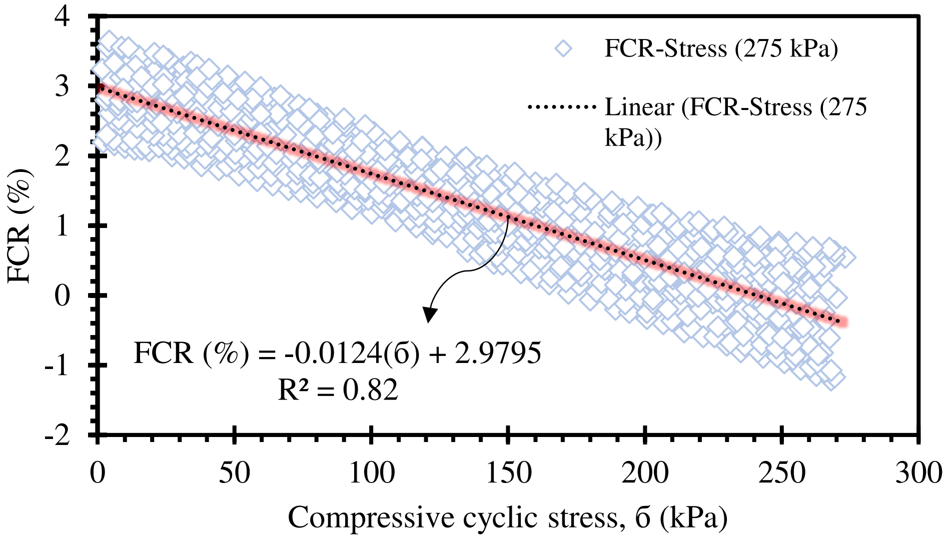
4
3
2
1
0
-1
-2
FCR (%)
0
50
100
150
200
250
300
Compressive cyclic stress, б (kPa)
FCR-Stress (275 kPa)
Linear (FCR-Stress (275 kPa))
FCR (%) = -0.0124(б) + 2.9795
R² = 0.82

(b)

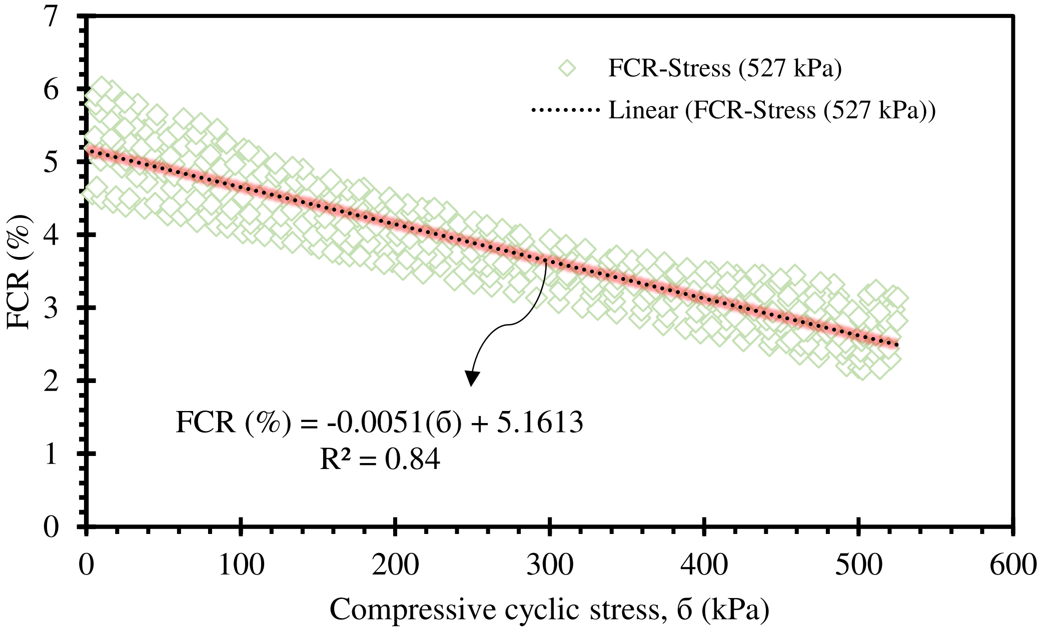
7
6
5
4
3
2
1
0
FCR (%)
0
100
200
300
400
500
600
Compressive cyclic stress, б (kPa)
FCR-Stress (527 kPa)
Linear (FCR-Stress (527 kPa))
FCR (%) = -0.0051(б) + 5.1613
R² = 0.84

(c)

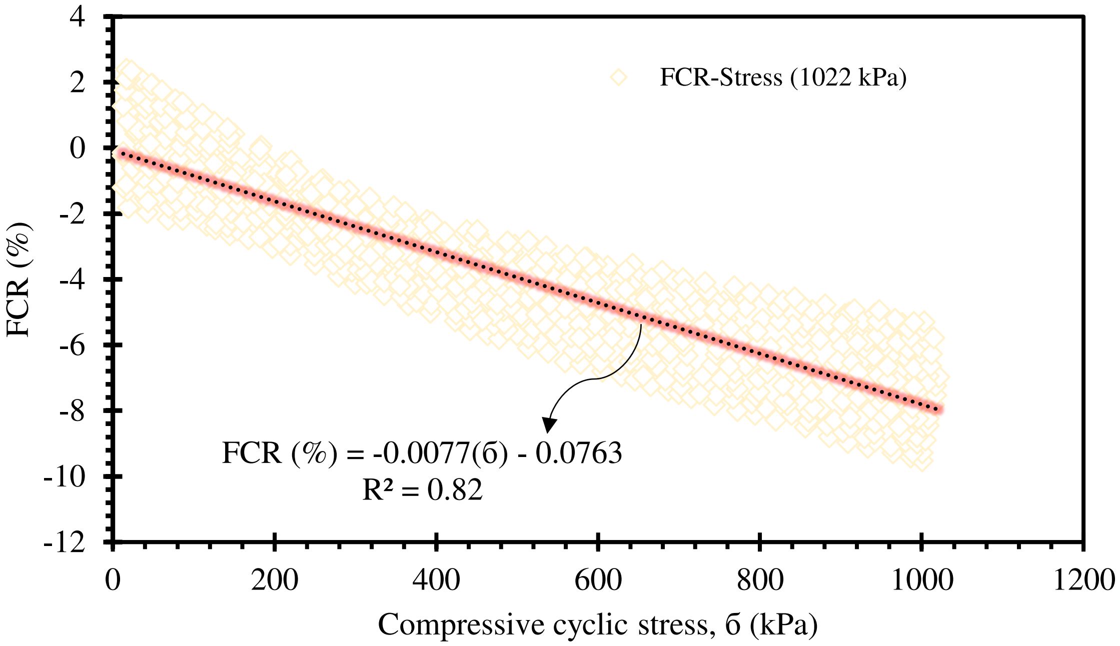

(d)

Figure 10. FCR-Stress relationship.

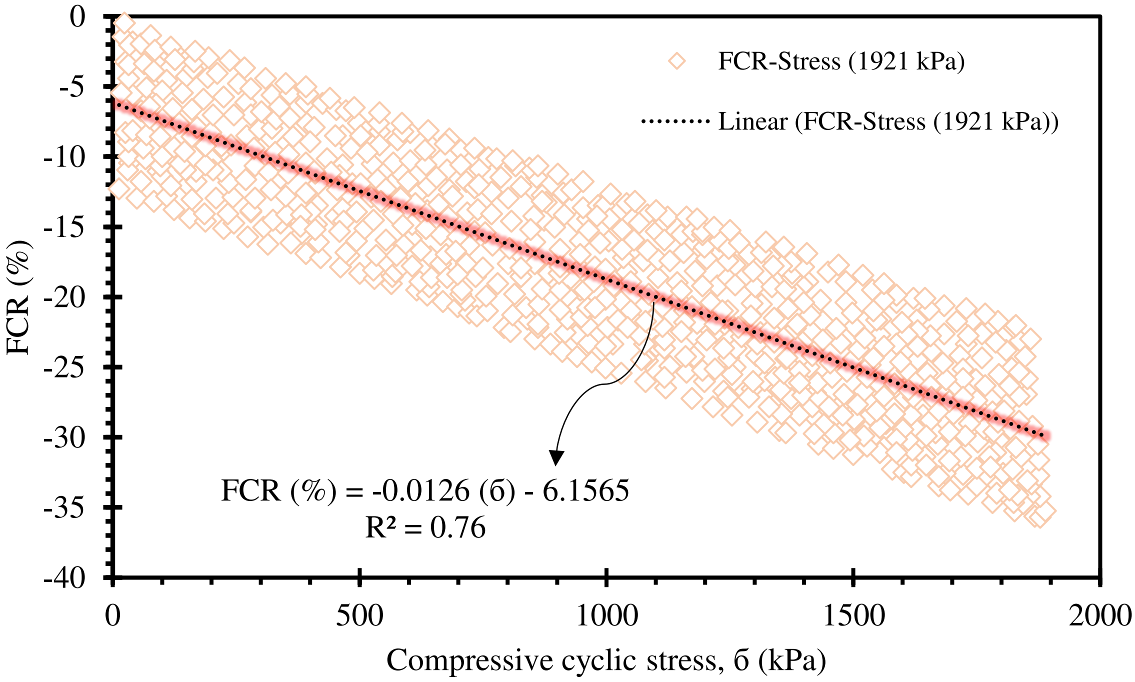

(a)

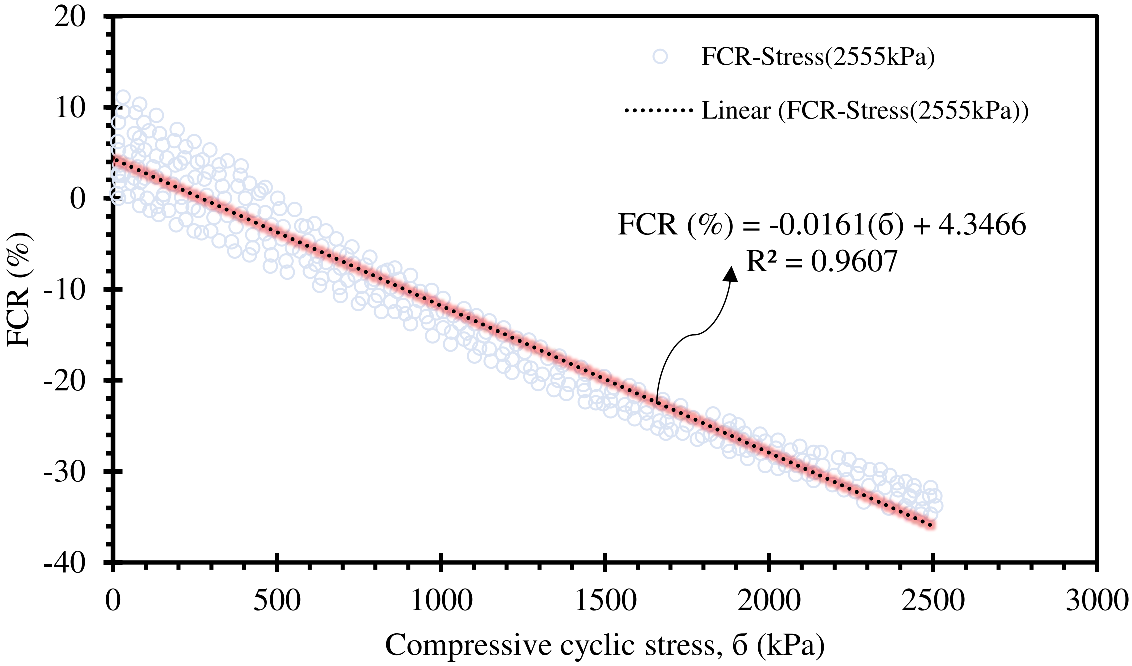
FCR-Stress(2555kPa)
Linear (FCR-Stress(2555kPa))
FCR (%) = -0.0161(б) + 4.3466
R² = 0.9607
FCR (%)
20
10
0
-10
-20
-30
-40
0
500
1000
1500
2000
2500
3000
Compressive cyclic stress, б (kPa)

(b)

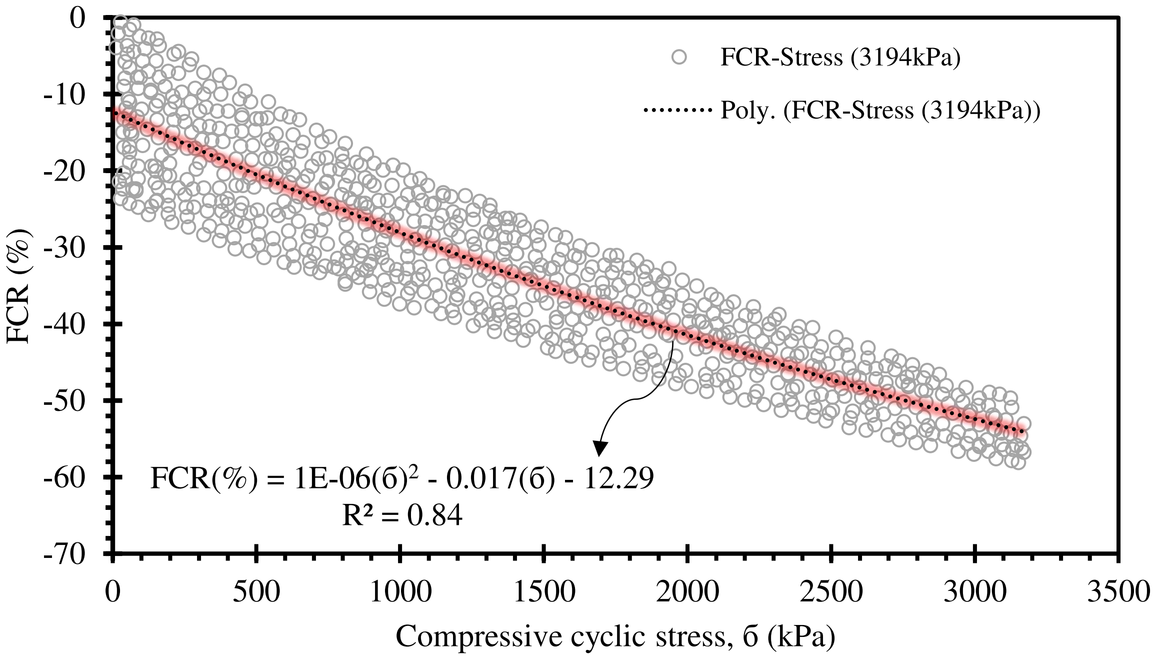
FCR-Stress (3194kPa)
Poly. (FCR-Stress (3194kPa))
FCR(%) = 1E-06(б)² - 0.017(б) - 12.29
R² = 0.84
FCR (%)
0
-10
-20
-30
-40
-50
-60
-70
0
500
1000
1500
2000
2500
3000
3500
Compressive cyclic stress, б (kPa)

(c)

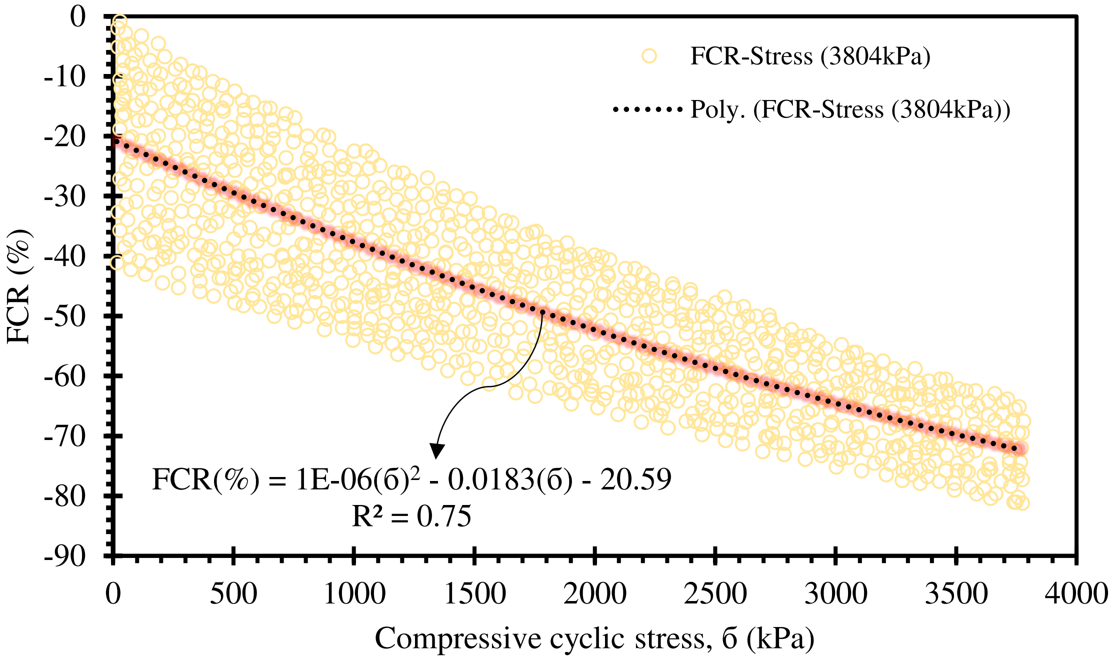

(d)

Figure 11. FCR-Stress relationship.

3.5. Microstructure analysis

The morphologies of the MWCNTs and graphene nanoplatelets are illustrated in Figures 12a and b, respectively. MWCNTs composed of buckytubes are two-dimensional and form a hollow structure. Figure 12a indicates a high aspect ratio (length/diameter) for MWCNTs; thus, this high aspect ratio results in bridging effects in cementitious composites. The bridging effects of MWCNTs increase the electrical conductivity between cementitious composites and mechanical strength [81]. Figure 12b presents the microstructure of the graphene nanoplatelets (GNP) utilized in this study. The GNPs are lightweight and have a low density, excellent mechanical characteristics, high specific surface area, and electrical conduction characteristics. Given these features, adding GNPs to cement-stabilized sand increases the electrical conductivity and mechanical strength.

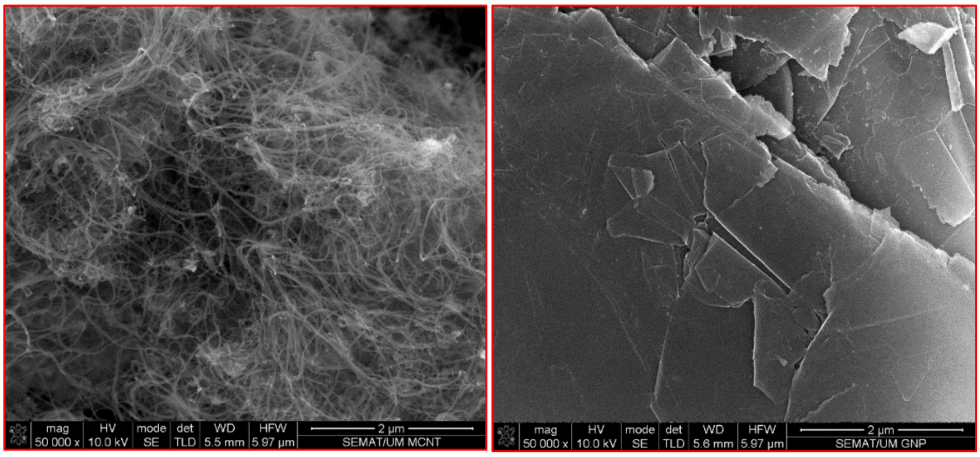

(a) (b)

Figure 12. Morphology of a) MWCNTs and b) GNPs.

As discussed earlier, the piezoresistive performance of the self-sensing cementitious composite depends on loading conditions based on the electrode location used for recording the electrical resistance. To analyse this issue according to the microstructure condition, the 1 cm^3 samples for SEM analysis were provided from two locations, under the loading region and outside of the loading region, as seen in Figures 13a and b. After electromechanical testing, the first sample shown in Figure 13a was prepared from the region directly subjected to loading. In contrast, the sample shown in Figure 13b was provided from the location outside of the loading region.

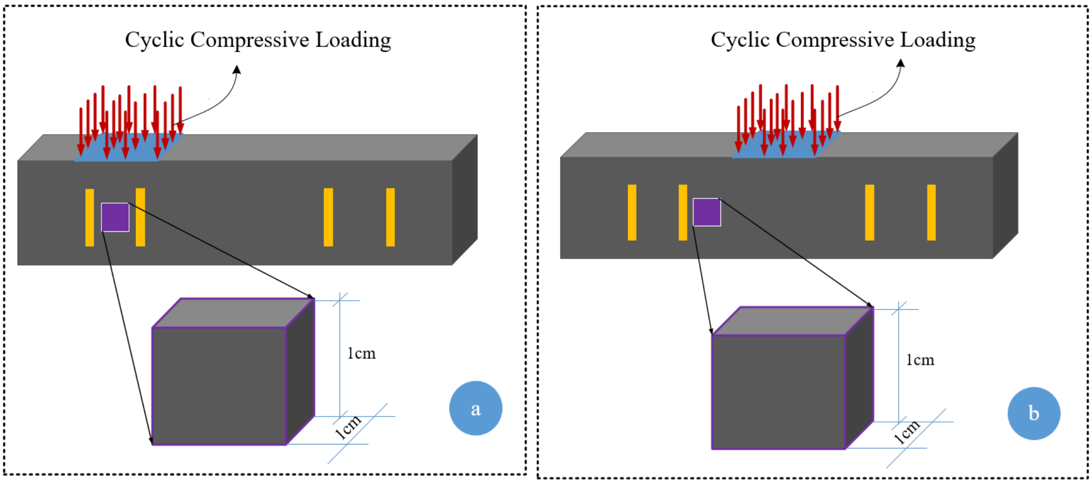

Figure 13. Location of sampling for microstructural analysis after electromechanical testing.

The existing pores in the self-sensing cementitious composite represent one of the main influential factors affecting the piezoresistive performance [82]. Thus, the variation in electrical resistance with regard to loading conditions could be clearly explained through SEM morphologies. The microstructural features of the sample prepared from the region under loading (see Figure 12a) are shown in Figure 14. On the other hand, the microstructural features of the sample taken from the region outside of the loading area (see Figure 13b) are presented in Figure 15. The pores and voids shown in black spots in Figure 14 are smaller than those in Figure 15. Therefore, comparing Figures 14 and 15 indicates the densified microstructures for the sample provided from the region under loading (Figure 14) compared to the sample taken from a region outside the loading area (Figure 15). The higher stress sensitivity of self-sensing cement-stabilized sand in the loading condition on top of electrodes could be due to the compacted and densified microstructure that emerged upon loading. Given this issue, when the electrical resistance is recorded from the electrodes covered by the loading area, the piezoresistive performance of self-sensing is considerable compared to the case in which the electrical resistance is recorded using the electrodes outside of the loading area.

The cement hydration and pozzolanic reactions produce calcium silicate hydrate (CSH) and calcium aluminate hydrate (CAH), leading to the strength gain of calcium-based stabilized geomaterials [83,84], particularly cement-stabilized composites [85,86]. A previous study's findings showed that cement hydration products fully adhere to the surface of carbon nanomaterials [87]. The adhesion of cement hydration products on the surface of carbon nanomaterials is due to a considerably large specific surface area and high surface energy [88]. Given this issue, the MWCNT/GNP bridges the pores and cement hydration products, resulting in conductive pathways. In the portion of the sample subjected directly to loading, the bridging effects of MWCNT/GNP accumulate further, as seen in Figure 14. In contrast, the bridging effects of MWCNT/GNP outside the loading region remain unchanged or decrease due to tension, as can be observed in Figure 15. Therefore, resistance variation occurs in the self-sensing cement-stabilized samples, resulting in different sensitivity responses to the loading conditions.

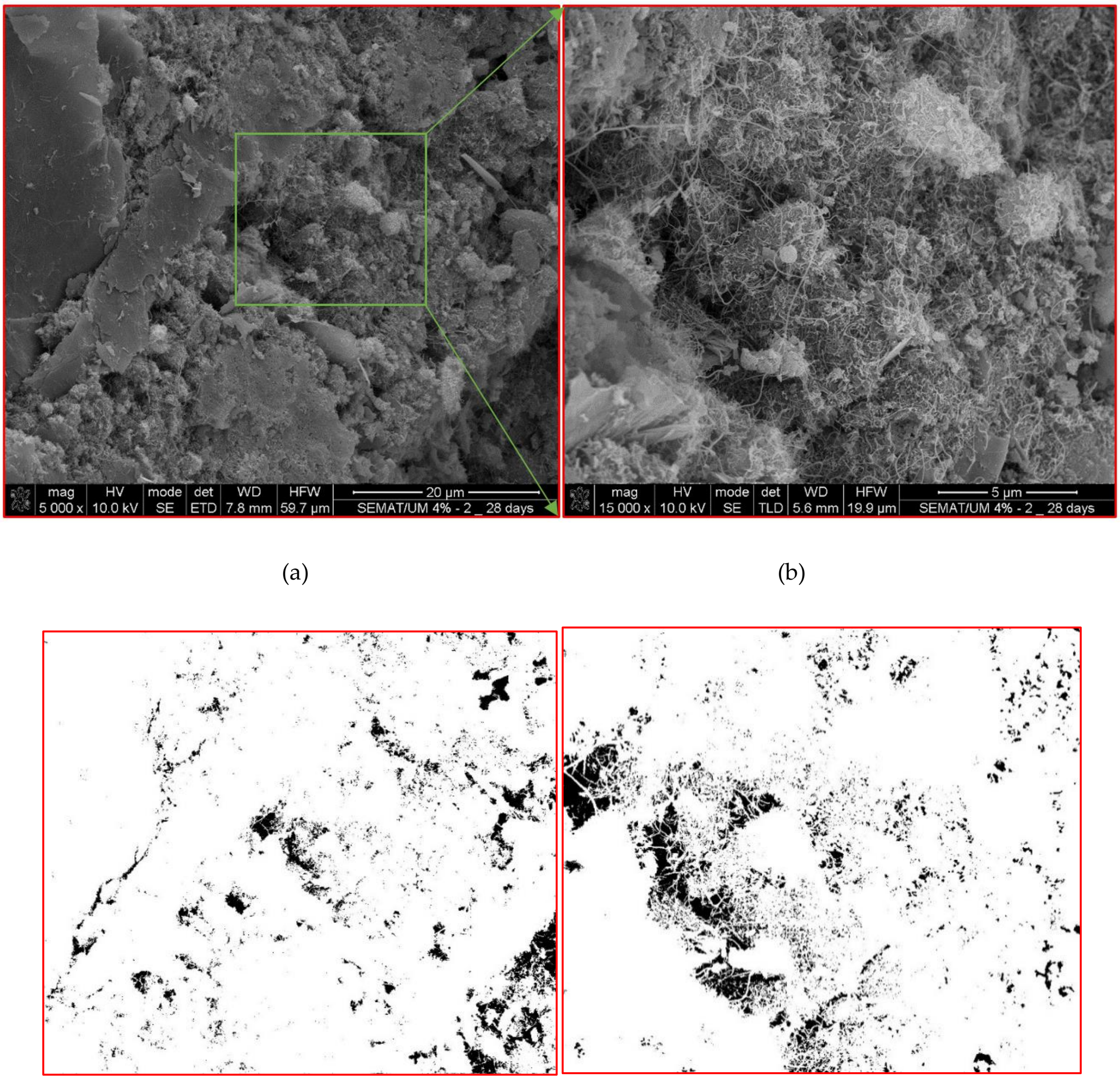

(a) (b)

(c) (d)

Figure 14. Microstructure of self-sensing cementitious composite sampled from the under loading region according to Figure 12a.

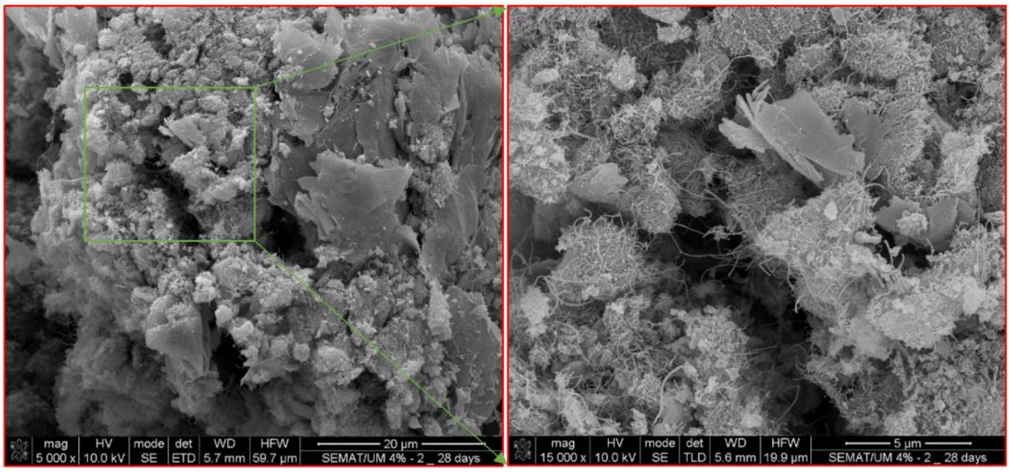

(a) (b)

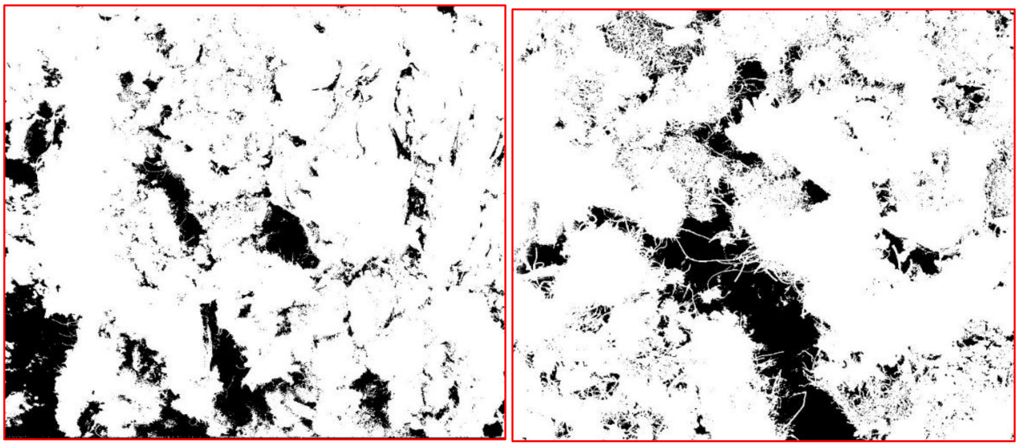

(c) (d)

Figure 15. Microstructure of self-sensing cementitious composite sampled from outside the loading region according to Figure 12b.

To further analyse the effects of microstructures on the sensitivity of cement-stabilized sand with regard to loading conditions, a schematic illustration shown in Figure 16 is considered. Figure 16 exhibits a schematic illustration of the microstructure condition under loading on top of two electrodes (electrodes 1 and 2). The micro- and nanovoids decrease under compressive loading. In contrast, the effects of loading on the microstructure compression decrease with increasing distance from the loading area, as shown in Figure 16. Given this phenomenon, when the specimen is loaded on a specific surface, the resistance of self-sensing cement-stabilized sand under loading is not homogeneous through whole samples. Depending on the location of the loading area, the electrical resistance differs. For instance, the electrical resistance of the portion directly subjected to loading (R_u) is smaller than that of regions far from the loading area (R_o), as illustrated in Figure 16. Therefore, the piezoresistive performance of self-sensing cement-stabilized sand substantially depends on the electrode location used for electrical resistance recording. For instance, considering the two-electrode probe system circuit, the electrical resistance in Figure 16 could be recorded using different connection options between electrodes (i.e., 1-2; 1-3; 1-4; 2-3; and 2-4 options). Regarding Figure 16, the piezoresistive performance of self-sensing cement-stabilized sand would be considerable if the electrical resistance is recorded using electrodes 1 and 2 (1-2 option) compared to cases in which the electrical resistance is recorded using other electrode layout options (1-3; 1-4; 2-3; and 2-4). This issue is attributed to densified and loose microstructures occurring under the loading region and outside of the loading regions, respectively, as seen in Figures 14 and 15.

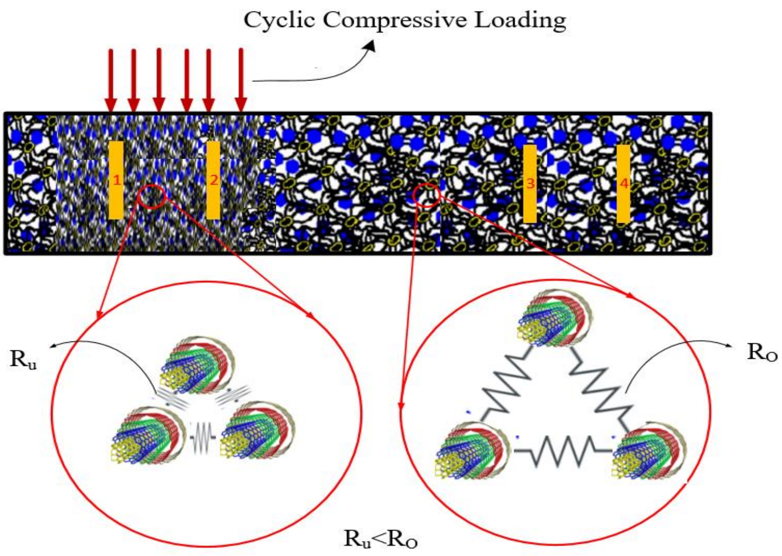

Figure 16. Schematic illustration of the microstructure of the self-sensing cementitious composite of the under loading region (R_u) and out-of-loading region (R_o).

4. Conclusions

The influences of various cyclic compressive loading conditions on the electromechanical performance of self-sensing cement-stabilized sand were evaluated. In addition, SEM was conducted to explore the effects of loading conditions on the morphological features of self-sensing cement-stabilized sand. Based on the experimental findings, the following conclusions are drawn:

1. The distance between electrodes used for electrical resistance recording considerably affects sensitivity.
2. The distance of the loading region from the electrodes employed for electrical resistance recording considerably affects the electromechanical performance of cement-stabilized sand.
3. Depending on the location of electrodes relative to the loading region, the self-sensing cement-stabilized sand yielded various performances under the same stress level. The best sensitivity was observed when the electrodes were located directly under the loading region.
4. The FCR increased with increasing stress level, showing the enhanced sensitivity of self-sensing cement-stabilized sand with increasing stress level. However, the reversibility decreases when the applied stress level is more than 67% of the ultimate strength of cement-stabilized sand.
5. The FCR suddenly decreased under the few cycles of the applied low stress level (63 kPa), and then it became constant under subsequent cycles of the same stress level. This issue can be attributed to the effects of accommodation that occurred under the first few cycles. Therefore, the accommodation effects at the beginning of loading must be considered for calibrating self-sensing cement-stabilized sand performance.
6. The SEM results yielded the accumulated bridging effects of carbon nanomaterials under the loading region and weakened bridging effects outside the loading region. Therefore, the considerable sensitivity of self-sensing cement-stabilized sand under the loading condition directly on top of electrodes may be due to accumulated bridging effects of carbon nonmaterial that could provide random conductive networks.

The findings have presented the effects of loading conditions and level on the electromechanical performance of self-sensing cement-stabilized sand. The findings indicate the crucial role of electrode layout on the sensing performance of cement-stabilized sand that needs to be considered before applying this smart material in civil engineering projects.

CRediT authorship contribution statement: Mohammad Jawed Roshan: Conceptualization, methodology, writing original draft, preparation, validation, formal analysis, investigation, data curation, writing review and editing, visualization; **Mohammadmahdi Abedi:** Conceptualization, methodology, writing review and

editing; **António Gomes Correia:** Conceptualization, methodology, validation, formal analysis, investigation, resources, data curation, writing review and editing, visualization, supervision, project administration, funding acquisition; **Raul Fangueiro:** Conceptualization, methodology, validation, formal analysis, investigation, resources, data curation, writing review and editing, visualization, supervision, project administration, funding acquisition

Data Availability: The datasets used or analysed during the current study are available from the corresponding author on reasonable request.

Acknowledgements: This work was supported by the European Commission-Shift2Rail Program under the project "IN2TRACK3, H2020–S2RJU-CFM-2020, S2R-CFMIP3- 01–2020". Furthermore, this work was partly financed by FCT / MCTES through national funds (PIDDAC), under the R&D Unit Institute for Sustainability and Innovation in Structural Engineering (ISISE), under reference UIDB / 04029/2020, under project UID/QUI/00686/2020 of CQ, and also under the Associate Laboratory Advanced Production and Intelligent Systems ARISE under reference LA/P/0112/2020, as well as under the R&D Unit of the Centre for Textile Science and Technology (2C2T). The first author also acknowledges the individual research fellowship provided by the FCT with reference number of "2023.03777.BD".

Declaration of Competing Interest: The authors declare no conflict of interest.

References

1. Razali, R.; Rashid, A.S.A.; Hezmi, M.A.; Roshan, M.J.; Zakaria, N.S.S.; Lat, D.C.; Rahman, N.S.A. Experimental Study on Mechanical Behavior of Laterite Soil Treated with Quicklime. *J. Mech. Eng.* **2022**, *11*, 109–122.
2. Tamassoki, S.; Nik Daud, N.N.; Nejabi, M.N.; Roshan, M.J. Fibre-Reinforced Soil Mixed Lime/Cement Additives: A Review. *Pertanika J. Sci. Technol.* **2022**, *31*, 217–235, doi:10.47836/pjst.31.1.14.
3. Alnedawi, A.; Ullah, S.; Azam, A.; Mousa, E.; Obaid, I.; Yosri, A. Integrated and Holistic Knowledge Map of Resilient Modulus Studies for Pavement Materials: A Scientometric Analysis and Bibliometric Review of Research Frontiers and Prospects. *Transp. Geotech.* **2022**, *33*, 100711, doi:10.1016/j.trgeo.2021.100711.
4. Nalon, G.H.; Santos, R.F.; Lima, G.E.S. de; Andrade, I.K.R.; Pedroti, L.G.; Ribeiro, J.C.L.; Franco de Carvalho, J.M. Recycling Waste Materials to Produce Self-Sensing Concretes for Smart and Sustainable Structures: A Review. *Constr. Build. Mater.* **2022**, *325*, 126658, doi:10.1016/j.conbuildmat.2022.126658.
5. Shi, L.; Lu, Y.; Bai, Y. Mechanical and Electrical Characterisation of Steel Fiber and Carbon Black Engineered Cementitious Composites. *Procedia Eng.* **2017**, *188*, 325–332, doi:10.1016/j.proeng.2017.04.491.
6. Ding, Y.; Li, D.; Ma, Y.; Liu, G.; Song, S.; Zhang, D.; Ding, G. Self-Localization of the Flexural Cracks of Fiber Reinforced Concrete Beams. *Constr. Build. Mater.* **2021**, *302*, 124364, doi:10.1016/j.conbuildmat.2021.124364.
7. Demircilioglu, E.; Teomete, E.; Ozbulut, O.E. Strain Sensitivity of Steel-Fiber-Reinforced Industrial Smart Concrete. *J. Intell. Mater. Syst. Struct.* **2020**, *31*, 127–136, doi:10.1177/1045389X19888722.
8. Wang, H.; Shi, F.; Shen, J.; Zhang, A.; Zhang, L.; Huang, H.; Liu, J.; Jin, K.; Feng, L.; Tang, Z. Research on the Self-Sensing and Mechanical Properties of Aligned Stainless Steel Fiber-Reinforced Reactive Powder Concrete. *Cem. Concr. Compos.* **2021**, *119*, 104001, doi:10.1016/j.cemconcomp.2021.104001.
9. Donnini, J.; Bellezze, T.; Corinaldesi, V. Mechanical, Electrical and Self-Sensing Properties of Cementitious Mortars Containing Short Carbon Fibers. *J. Build. Eng.* **2018**, *20*, 8–14, doi:10.1016/j.jobe.2018.06.011.
10. Galao, O.; Baeza, F.J.; Zornoza, E.; Garcés, P. Strain and Damage Sensing Properties on Multifunctional Cement Composites with CNF Admixture. *Cem. Concr. Compos.* **2014**, *46*, 90–98, doi:10.1016/j.cemconcomp.2013.11.009.
11. Azhari, F.; Banthia, N. Cement-Based Sensors with Carbon Fibers and Carbon Nanotubes for Piezoresistive Sensing. *Cem. Concr. Compos.* **2012**, *34*, 866–873, doi:10.1016/j.cemconcomp.2012.04.007.
12. Baeza, F.J.; Galao, O.; Zornoza, E.; Garcés, P. Effect of Aspect Ratio on Strain Sensing Capacity of Carbon Fiber Reinforced Cement Composites. *Mater. Des.* **2013**, *51*, 1085–1094, doi:10.1016/j.matdes.2013.05.010.
13. Huang, Y.; Li, H.; Qian, S. Self-Sensing Properties of Engineered Cementitious Composites. *Constr. Build. Mater.* **2018**, *174*, 253–262, doi:10.1016/j.conbuildmat.2018.04.129.
14. Al-Dahawi, A.; Sarwary, M.H.; Öztürk, O.; Yildirim, G.; Akin, A.; Şahmaran, M.; Lachemi, M. Electrical Percolation Threshold of Cementitious Composites Possessing Self-Sensing Functionality Incorporating Different Carbon-Based Materials. *Smart Mater. Struct.* **2016**, *25*, 105005, doi:10.1088/0964-1726/25/10/105005.
15. Monteiro, A.O.; Cachim, P.B.; Costa, P.M.F.J. Self-Sensing Piezoresistive Cement Composite Loaded with Carbon Black Particles. *Cem. Concr. Compos.* **2017**, *81*, 59–65, doi:10.1016/j.cemconcomp.2017.04.009.
16. Nalon, G.H.; Ribeiro, J.C.L.; Araújo, E.N.D. de; Pedroti, L.G.; Carvalho, J.M.F. de; Santos, R.F.; Aparecido-Ferreira, A. Effects of Different Kinds of Carbon Black Nanoparticles on the Piezoresistive and Mechanical Properties of Cement-Based Composites. *J. Build. Eng.* **2020**, *32*, 101724, doi:10.1016/j.jobe.2020.101724.

17. Dong, W.; Li, W.; Shen, L.; Sun, Z.; Sheng, D. Piezoresistivity of Smart Carbon Nanotubes (CNTs) Reinforced Cementitious Composite under Integrated Cyclic Compression and Impact. *Compos. Struct.* **2020**, *241*, 112106, doi:10.1016/j.compstruct.2020.112106.
18. Li, G.Y.; Wang, P.M.; Zhao, X. Pressure-Sensitive Properties and Microstructure of Carbon Nanotube Reinforced Cement Composites. *Cem. Concr. Compos.* **2007**, *29*, 377–382, doi:10.1016/j.cemconcomp.2006.12.011.
19. Parvaneh, V.; Khiabani, S.H. Mechanical and Piezoresistive Properties of Self-Sensing Smart Concretes Reinforced by Carbon Nanotubes. *Mech. Adv. Mater. Struct.* **2019**, *26*, 993–1000, doi:10.1080/15376494.2018.1432789.
20. Ding, S.; Xiang, Y.; Ni, Y.Q.; Thakur, V.K.; Wang, X.; Han, B.; Ou, J. In-Situ Synthesizing Carbon Nanotubes on Cement to Develop Self-Sensing Cementitious Composites for Smart High-Speed Rail Infrastructures. *Nano Today* **2022**, *43*, 101438, doi:10.1016/j.nantod.2022.101438.
21. Jang, D.; Yoon, H.N.; Farooq, S.Z.; Lee, H.K.; Nam, I.W. Influence of Water Ingress on the Electrical Properties and Electromechanical Sensing Capabilities of CNT/Cement Composites. *J. Build. Eng.* **2021**, *42*, 103065, doi:10.1016/j.jobe.2021.103065.
22. Qi, G.; Wang, Q.; Zhang, R.; Guo, Z.; Zhan, D.; Liu, S. Effect of RGO/GNP on the Electrical Conductivity and Piezoresistance of Cement-Based Composite Subjected to Dynamic Loading. *Constr. Build. Mater.* **2023**, *368*, 130340, doi:10.1016/j.conbuildmat.2023.130340.
23. Sevim, O.; Jiang, Z.; Ozbulut, O.E. Effects of Graphene Nanoplatelets Type on Self-Sensing Properties of Cement Mortar Composites. *Constr. Build. Mater.* **2022**, *359*, 129488, doi:10.1016/j.conbuildmat.2022.129488.
24. Dong, W.; Li, W.; Guo, Y.; Wang, K.; Sheng, D. Mechanical Properties and Piezoresistive Performances of Intrinsic Graphene Nanoplate/Cement-Based Sensors Subjected to Impact Load. *Constr. Build. Mater.* **2022**, *327*, 126978, doi:10.1016/j.conbuildmat.2022.126978.
25. Gulisano, F.; Abedi, M.; Jurado-Piña, R.; Apaza, F.R.A.; Roshan, M.J.; Fangueiro, R.; Correia, A.G.; Gallego, J. Stress and Damage-Sensing Capabilities of Asphalt Mixtures Incorporating Graphene Nanoplatelets. *Sensors Actuators A Phys.* **2023**, *359*, 114494, doi:10.1016/j.sna.2023.114494.
26. Belli, A.; Mobili, A.; Bellezze, T.; Cachim, P.B.; Tittarelli, F. Commercial and Recycled Carbon-Based Fillers and Fibers for Self-Sensing Cement-Based Composites: Comparison of Mechanical Strength, Durability, and Piezoresistive Behavior. *J. Build. Eng.* **2023**, *73*, 106836, doi:10.1016/j.jobe.2023.106836.
27. Gulisano, F.; Buasiri, T.; Apaza, F.R.A.; Cwirzen, A.; Gallego, J. Piezoresistive Behavior of Electric Arc Furnace Slag and Graphene Nanoplatelets Asphalt Mixtures for Self-Sensing Pavements. *Autom. Constr.* **2022**, *142*, 104534, doi:10.1016/j.autcon.2022.104534.
28. Kim, T.U.; Kim, M.K.; Park, J.W.; Kim, D.J. Effects of Temperature and Humidity on Self-Stress Sensing Capacity of Smart Concrete Blocks. *J. Build. Eng.* **2023**, *69*, 106227, doi:10.1016/j.jobe.2023.106227.
29. Wang, D.; Dong, S.; Wang, X.; Maimaitituersun, N.; Shao, S.; Yang, W.; Han, B. Sensing Performances of Hybrid Steel Wires and Fibers Reinforced Ultra-High Performance Concrete for in-Situ Monitoring of Infrastructures. *J. Build. Eng.* **2022**, *58*, 105022, doi:10.1016/j.jobe.2022.105022.
30. Roopa, A.K.; Hunashyal, A.M.; Mysore, R.R.M. Development and Implementation of Cement-Based Nanocomposite Sensors for Structural Health Monitoring Applications: Laboratory Investigations and Way Forward. *Sustain.* **2022**, *14*, 12452, doi:10.3390/su141912452.
31. Liu, X.; Wang, G.; Yu, J.; Liu, R.; Lyu, K.; Zuo, J.; Shah, S.P. Stress-Sensitivity of Carbon Nanotube-Grafted-Carbon Fiber Incorporated Cement-Based Composites. *J. Build. Eng.* **2023**, *64*, 105589, doi:10.1016/j.jobe.2022.105589.
32. Yıldırım, G.; Sarwary, M.H.; Al-Dahawi, A.; Öztürk, O.; Anıl, Ö.; Şahmaran, M. Piezoresistive Behavior of CF- and CNT-Based Reinforced Concrete Beams Subjected to Static Flexural Loading: Shear Failure Investigation. *Constr. Build. Mater.* **2018**, *168*, 266–279, doi:10.1016/j.conbuildmat.2018.02.124.
33. Yoo, D.-Y.; Kim, S.; Lee, S.H. Self-Sensing Capability of Ultra-High-Performance Concrete Containing Steel Fibers and Carbon Nanotubes under Tension. *Sensors Actuators A Phys.* **2018**, *276*, 125–136, doi:10.1016/j.sna.2018.04.009.
34. Kim, H.K.; Nam, I.W.; Lee, H.K. Enhanced Effect of Carbon Nanotube on Mechanical and Electrical Properties of Cement Composites by Incorporation of Silica Fume. *Compos. Struct.* **2014**, *107*, 60–69, doi:10.1016/j.compstruct.2013.07.042.
35. Wang, L.; Aslani, F. Piezoresistivity Performance of Cementitious Composites Containing Activated Carbon Powder, Nano Zinc Oxide and Carbon Fibre. *Constr. Build. Mater.* **2021**, *278*, 122375, doi:10.1016/j.conbuildmat.2021.122375.
36. Choi, K.; Min, Y.K.; Chung, W.; Lee, S.E.; Kang, S.W. Effects of Dispersants and Defoamers on the Enhanced Electrical Performance by Carbon Nanotube Networks Embedded in Cement-Matrix Composites. *Compos. Struct.* **2020**, *243*, 112193, doi:10.1016/j.compstruct.2020.112193.
37. Al-Dahawi, A.; Öztürk, O.; Emami, F.; Yildirim, G.; Şahmaran, M. Effect of Mixing Methods on the Electrical Properties of Cementitious Composites Incorporating Different Carbon-Based Materials. *Constr. Build. Mater.* **2016**, *104*, 160–168, doi:10.1016/j.conbuildmat.2015.12.072.

38. Yıldırım, G.; Öztürk, O.; Al-Dahawi, A.; Afşın Ulu, A.; Şahmaran, M. Self-Sensing Capability of Engineered Cementitious Composites: Effects of Aging and Loading Conditions. *Constr. Build. Mater.* **2020**, *231*, 117132, doi:10.1016/j.conbuildmat.2019.117132.
39. Zhan, M.; Pan, G.; Zhou, F.; Mi, R.; Shah, S.P. In Situ-Grown Carbon Nanotubes Enhanced Cement-Based Materials with Multifunctionality. *Cem. Concr. Compos.* **2020**, *108*, 103518, doi:10.1016/j.cemconcomp.2020.103518.
40. Deng, H.; Li, H. Assessment of Self-Sensing Capability of Carbon Black Engineered Cementitious Composites. *Constr. Build. Mater.* **2018**, *173*, 1–9, doi:10.1016/j.conbuildmat.2018.04.031.
41. Qiu, L.; Dong, S.; Yu, X.; Han, B. Self-Sensing Ultra-High Performance Concrete for in-Situ Monitoring. *Sensors Actuators A Phys.* **2021**, *331*, 113049, doi:10.1016/j.sna.2021.113049.
42. Meng, X.; Feng, J.; Pai, N.; Zequan, H.; Kaiyuan, L.; Cheng, Z.; Yazhen, Z. Effects of Filler Type and Aging on Self-Sensing Capacity of Cement Paste Using Eddy Current-Based Nondestructive Detection. *Meas. J. Int. Meas. Confed.* **2021**, *182*, 109708, doi:10.1016/j.measurement.2021.109708.
43. Ding, S.; Wang, Y.W.; Ni, Y.Q.; Han, B. Structural Modal Identification and Health Monitoring of Building Structures Using Self-Sensing Cementitious Composites. *Smart Mater. Struct.* **2020**, *29*, 055013, doi:10.1088/1361-665X/ab79b9.
44. Sun, M.Q.; Liew, R.J.Y.; Zhang, M.H.; Li, W. Development of Cement-Based Strain Sensor for Health Monitoring of Ultra High Strength Concrete. *Constr. Build. Mater.* **2014**, *65*, 630–637, doi:10.1016/j.conbuildmat.2014.04.105.
45. Han, J.; Pan, J.; Ma, X.; Cai, J. Sensing Performance of Engineered Cementitious Composites in Different Application Forms. *Constr. Build. Mater.* **2022**, *355*, 129223, doi:10.1016/j.conbuildmat.2022.129223.
46. Wu, S.; Dai, H.; Wang, W. Effect of CFRC Layers on the Electrical Properties and Failure Mode of RC Beams Strengthened with CFRC Composites. *Smart Mater. Struct.* **2007**, *16*, 2056–2062, doi:10.1088/0964-1726/16/6/008.
47. Ding, S.; Ruan, Y.; Yu, X.; Han, B.; Ni, Y.-Q. Self-Monitoring of Smart Concrete Column Incorporating CNT/NCB Composite Fillers Modified Cementitious Sensors. *Constr. Build. Mater.* **2019**, *201*, 127–137, doi:10.1016/j.conbuildmat.2018.12.203.
48. Dong, W.; Li, W.; Zhu, X.; Sheng, D.; Shah, S.P. Multifunctional Cementitious Composites with Integrated Self-Sensing and Hydrophobic Capacities toward Smart Structural Health Monitoring. *Cem. Concr. Compos.* **2021**, *118*, 103962, doi:10.1016/j.cemconcomp.2021.103962.
49. Suo, Y.; Xia, H.; Guo, R.; Yang, Y. Study on Self-Sensing Capabilities of Smart Cements Filled with Graphene Oxide under Dynamic Cyclic Loading. *J. Build. Eng.* **2022**, *58*, 104775, doi:10.1016/j.jobe.2022.104775.
50. Al-Dahawi, A.; Yıldırım, G.; Öztürk, O.; Şahmaran, M. Assessment of Self-Sensing Capability of Engineered Cementitious Composites within the Elastic and Plastic Ranges of Cyclic Flexural Loading. *Constr. Build. Mater.* **2017**, *145*, 1–10, doi:10.1016/j.conbuildmat.2017.03.236.
51. Jawed Roshan, M.; Abedi, M.; Gomes Correia, A.; Fangueiro, R. Application of Self-Sensing Cement-Stabilized Sand for Damage Detection. *Constr. Build. Mater.* **2023**, *403*, 133080, doi:10.1016/j.conbuildmat.2023.133080.
52. Ullah, R.; Abdullah, R.A.; Kassim, A.; Yunus, N.Z.M.; Ullah, A.; Junaid, M.; Roshan, M.J. Effectiveness of Laser Diffraction Method for Particle Size Evaluation of Residual Soil. *Indian Geotech. J.* **2022**, *52*, 1476–1486, doi:10.1007/s40098-022-00615-1.
53. Dunuweera, S.P.; Rajapakse, R.M.G. Cement Types, Composition, Uses and Advantages of Nanocement, Environmental Impact on Cement Production, and Possible Solutions. *Adv. Mater. Sci. Eng.* **2018**, *2018*, 1–11, doi:10.1155/2018/4158682.
54. Roshan, M.J.; A Rashid, A.S.; Abdul Wahab, N.; Tamassoki, S.; Jusoh, S.N.; Hezmi, M.A.; Nik Daud, N.N.; Mohd Apandi, N.; Azmi, M. Improved Methods to Prevent Railway Embankment Failure and Subgrade Degradation: A Review. *Transp. Geotech.* **2022**, *37*, 100834, doi:10.1016/j.trgeo.2022.100834.
55. Han, B.; Ding, S.; Yu, X. Intrinsic Self-Sensing Concrete and Structures: A Review. *Meas. J. Int. Meas. Confed.* **2015**, *59*, 110–128, doi:10.1016/j.measurement.2014.09.048.
56. D'Alessandro, A.; Ubertini, F.; García-Macías, E.; Castro-Triguero, R.; Downey, A.; Laflamme, S.; Meoni, A.; Materazzi, A.L. Static and Dynamic Strain Monitoring of Reinforced Concrete Components through Embedded Carbon Nanotube Cement-Based Sensors. *Shock Vib.* **2017**, *2017*, 1–11, doi:10.1155/2017/3648403.
57. Parveen, S.; Rana, S.; Fangueiro, R.; Paiva, M.C. Microstructure and Mechanical Properties of Carbon Nanotube Reinforced Cementitious Composites Developed Using a Novel Dispersion Technique. *Cem. Concr. Res.* **2015**, *73*, 215–227, doi:10.1016/j.cemconres.2015.03.006.
58. Khushnood, R.A.; Arif, A.; Shaheen, N.; Zafar, A.G.; Hassan, T.; Akif, M. Bio-Inspired Self-Healing and Self-Sensing Cementitious Mortar Using Bacillus Subtilis Immobilized on Graphitic Platelets. *Constr. Build. Mater.* **2022**, *316*, 125818, doi:10.1016/j.conbuildmat.2021.125818.

59. Wang, Y.; Zhang, L. Development of Self-Sensing Cementitious Composite Incorporating Hybrid Graphene Nanoplates and Carbon Nanotubes for Structural Health Monitoring. *Sensors Actuators A Phys.* **2022**, *336*, 113367, doi:10.1016/j.sna.2022.113367.
60. Qiu, L.; Ding, S.; Wang, D.; Han, B. Self-Sensing GFRP-Reinforced Concrete Beams Containing Carbon Nanotube-Nano Carbon Black Composite Fillers. *Meas. Sci. Technol.* **2023**, *34*, 084003, doi:10.1088/1361-6501/accc20.
61. del Moral, B.; Baeza, F.J.; Navarro, R.; Galao, O.; Zornoza, E.; Vera, J.; Farcas, C.; Garcés, P. Temperature and Humidity Influence on the Strain Sensing Performance of Hybrid Carbon Nanotubes and Graphite Cement Composites. *Constr. Build. Mater.* **2021**, *284*, 122786, doi:10.1016/j.conbuildmat.2021.122786.
62. Xin, X.; Liang, M.; Yao, Z.; Su, L.; Zhang, J.; Li, P.; Sun, C.; Jiang, H. Self-Sensing Behavior and Mechanical Properties of Carbon Nanotubes/Epoxy Resin Composite for Asphalt Pavement Strain Monitoring. *Constr. Build. Mater.* **2020**, *257*, 119404, doi:10.1016/j.conbuildmat.2020.119404.
63. Wang, X.; Cao, B.; Vlachakis, C.; Al-Tabbaa, A.; Haigh, S.K. Characterization and Piezo-Resistivity Studies on Graphite-Enabled Self-Sensing Cementitious Composites with High Stress and Strain Sensitivity. *Cem. Concr. Compos.* **2023**, *142*, 105187, doi:10.1016/j.cemconcomp.2023.105187.
64. Yin, T.; Xu, J.; Wang, Y.; Liu, L. Increasing Self-Sensing Capability of Carbon Nanotubes Cement-Based Materials by Simultaneous Addition of Ni Nanofibers with Low Content. *Constr. Build. Mater.* **2020**, *254*, 119306, doi:10.1016/j.conbuildmat.2020.119306.
65. Wang, Y.; Sun, S.; Zhang, L. Self-Sensing Cementitious Composites Incorporating Hybrid NGPs/CNTs/NCBs for Structural Health Monitoring. *Sensors Actuators A Phys.* **2023**, *357*, 114365, doi:10.1016/j.sna.2023.114365.
66. Monteiro, A.O.; Loredo, A.; Costa, P.M.F.J.; Oeser, M.; Cachim, P.B. A Pressure-Sensitive Carbon Black Cement Composite for Traffic Monitoring. *Constr. Build. Mater.* **2017**, *154*, 1079–1086, doi:10.1016/j.conbuildmat.2017.08.053.
67. Wang, L.; Zhang, Y.; Du, H.; Feng, G.; Qi, T. Health Monitoring of C60 Smart Concrete Based on Self-Sensing. *Mater. Today Commun.* **2023**, *35*, 105834, doi:10.1016/j.mtcomm.2023.105834.
68. Kim, H.K.; Park, I.S.; Lee, H.K. Improved Piezoresistive Sensitivity and Stability of CNT/Cement Mortar Composites with Low Water-Binder Ratio. *Compos. Struct.* **2014**, *116*, 713–719, doi:10.1016/j.compstruct.2014.06.007.
69. Xu, C.; Fu, J.; Sun, L.; Masuya, H.; Zhang, L. Fatigue Damage Self-Sensing of Bridge Deck Component with Built-in Giant Piezoresistive Cementitious Carbon Fiber Composites. *Compos. Struct.* **2021**, *276*, 114459, doi:10.1016/j.compstruct.2021.114459.
70. Borke Birgin, H.; D'Alessandro, A.; Favaro, M.; Sangiorgi, C.; Laflamme, S.; Ubertini, F. Field Investigation of Novel Self-Sensing Asphalt Pavement for Weigh-in-Motion Sensing. *Smart Mater. Struct.* **2022**, *31*, 085004, doi:10.1088/1361-665X/ac7922.
71. Dong, W.; Li, W.; Guo, Y.; Sun, Z.; Qu, F.; Liang, R.; Shah, S.P. Application of Intrinsic Cement-Based Sensor for Traffic Detections of Human Motion and Vehicle Speed. *Constr. Build. Mater.* **2022**, *355*, 129130, doi:10.1016/j.conbuildmat.2022.129130.
72. Han, B.; Zhang, K.; Burnham, T.; Kwon, E.; Yu, X. Integration and Road Tests of a Self-Sensing CNT Concrete Pavement System for Traffic Detection. *Smart Mater. Struct.* **2013**, *22*, 015020, doi:10.1088/0964-1726/22/1/015020.
73. Han, B.; Wang, Y.; Ding, S.; Yu, X.; Zhang, L.; Li, Z.; Ou, J. Self-Sensing Cementitious Composites Incorporated with Botryoid Hybrid Nano-Carbon Materials for Smart Infrastructures. *J. Intell. Mater. Syst. Struct.* **2017**, *28*, 699–727, doi:10.1177/1045389X16657416.
74. Rao, R.K.; Sindu, B.S.; Sasmal, S. Real-Time Monitoring of Structures under Extreme Loading Using Smart Composite-Based Embeddable Sensors. *J. Intell. Mater. Syst. Struct.* **2022**, *34*, 1073–1096, doi:10.1177/1045389X221128586.
75. Dong, W.; Li, W.; Wang, K.; Luo, Z.; Sheng, D. Self-Sensing Capabilities of Cement-Based Sensor with Layer-Distributed Conductive Rubber Fibres. *Sensors Actuators A Phys.* **2020**, *301*, 111763, doi:10.1016/j.sna.2019.111763.
76. Ding, S.; Xu, C.; Ni, Y.Q.; Han, B. Extracting Piezoresistive Response of Self-Sensing Cementitious Composites under Temperature Effect via Bayesian Blind Source Separation. *Smart Mater. Struct.* **2021**, *30*, 065010, doi:10.1088/1361-665X/abf992.
77. Roshan, M.J.; Abedi, M.; Fangueiro, R.; Correia, A.G.; Silva, M.M. Evaluation Procedure for Damage Detection by a Self-Sensing Cement Composite. *Measurement* **2024**, *226*, 114149, doi:10.1016/j.measurement.2024.114149.
78. Wang, L.; Aslani, F. Self-Sensing Performance of Cementitious Composites with Functional Fillers at Macro, Micro and Nano Scales. *Constr. Build. Mater.* **2022**, *314*, 125679, doi:10.1016/j.conbuildmat.2021.125679.
79. Yoo, D.Y.; You, I.; Youn, H.; Lee, S.J. Electrical and Piezoresistive Properties of Cement Composites with Carbon Nanomaterials. *J. Compos. Mater.* **2018**, *52*, 3325–3340, doi:10.1177/0021998318764809.

80. Han, B.; Yu, X.; Ou, J. Sensing Properties of Self-Sensing Concrete. In *Self-Sensing Concrete in Smart Structures*; Elsevier, 2014; pp. 95–162 ISBN 9780128005170.
81. Yesudhas Jayakumari, B.; Nattanmai Swaminathan, E.; Partheeban, P. A Review on Characteristics Studies on Carbon Nanotubes-Based Cement Concrete. *Constr. Build. Mater.* **2023**, *367*, 130344, doi:10.1016/j.conbuildmat.2023.130344.
82. Kim, G.M.; Yang, B.J.; Cho, K.J.; Kim, E.M.; Lee, H.K. Influences of CNT Dispersion and Pore Characteristics on the Electrical Performance of Cementitious Composites. *Compos. Struct.* **2017**, *164*, 32–42, doi:10.1016/j.compstruct.2016.12.049.
83. Tamassoki, S.; Daud, N.N.N.; Jakarni, F.M.; Kusin, F.M.; Rashid, A.S.A.; Roshan, M.J. Compressive and Shear Strengths of Coir Fibre Reinforced Activated Carbon Stabilised Lateritic Soil. *Sustainability* **2022**, *14*, 9100, doi:10.3390/su14159100.
84. Tamassoki, S.; Nik Daud, N.N.; Jakarni, F.M.; Mohd Kusin, F.; Rashid, A.S.A.; Roshan, M.J. Performance Evaluation of Lateritic Subgrade Soil Treated with Lime and Coir Fibre-Activated Carbon. *Appl. Sci.* **2022**, *12*, 8279, doi:10.3390/app12168279.
85. Roshan, M.J.; Rashid, A.S.B.A.; Hezmi, M.A. Bin; Nejabi, M.N.; Siti, S.N.; Tamassoki, S.; Razali, R. Evaluation of Cement Stabilised Residual Soil on Macro- and Micro-Scale for Road Construction. *J. Eng. Appl. Sci.* **2022**, *69*, 109, doi:10.1186/s44147-022-00165-6.
86. Wahab, N.A.; Roshan, M.J.; Rashid, A.S.A.; Hezmi, M.A.; Jusoh, S.N.; Norsyahariati, N.D.N.; Tamassoki, S. Strength and Durability of Cement-Treated Lateritic Soil. *Sustain.* **2021**, *13*, 6430, doi:10.3390/su13116430.
87. Mardani, M.; Hossein Hosseini Lavassani, S.; Adresi, M.; Rashidi, A. Piezoresistivity and Mechanical Properties of Self-Sensing CNT Cementitious Nanocomposites: Optimizing the Effects of CNT Dispersion and Surfactants. *Constr. Build. Mater.* **2022**, *349*, 128127, doi:10.1016/j.conbuildmat.2022.128127.
88. Zhang, L.W.; Kai, M.F.; Liew, K.M. Evaluation of Microstructure and Mechanical Performance of CNT-Reinforced Cementitious Composites at Elevated Temperatures. *Compos. Part A Appl. Sci. Manuf.* **2017**, *95*, 286–293, doi:10.1016/j.compositesa.2017.02.001.